







RESEARCH PAPER



Novel tacrine–benzofuran hybrids as potential multi-target drug candidates for the treatment of Alzheimer’s Disease

Gaia Fancellu^{a,b,*} , Karam Chand^{a,*} , Daniel Tomás^a , Elisabetta Orlandini^b , Luca Piemontese^c , Diana F. Silva^d , Sandra M. Cardoso^{d,e} , Sílvia Chaves^a  and M. Amélia Santos^a 

^aCentro de Química Estrutural, Instituto Superior Técnico, Universidade de Lisboa, Lisboa, Portugal; ^bDepartment of Earth Sciences, University of Pisa, Pisa, Italy; ^cDipartimento di Farmacia–Scienze del Farmaco, Università degli Studi di Bari “Aldo Moro”, Bari, Italy; ^dCNC–Center for Neuroscience and Cell Biology, Universidade de Coimbra, Coimbra, Portugal; ^eInstitute of Molecular and Cell Biology, Faculty of Medicine, Universidade de Coimbra, Coimbra, Portugal

ABSTRACT

Pursuing the widespread interest on multi-target drugs to combat Alzheimer’s disease (AD), a new series of hybrids was designed and developed based on the repositioning of the well-known acetylcholinesterase (AChE) inhibitor, tacrine (TAC), by its coupling to benzofuran (BF) derivatives. The BF framework aims to endow the conjugate molecules with ability for inhibition of AChE (bimodal way) and of amyloid-beta peptide aggregation, besides providing metal (Fe, Cu) chelating ability and concomitant extra anti-oxidant activity, for the hybrids with hydroxyl substitution. The new TAC-BF conjugates showed very good activity for AChE inhibition (sub-micromolar range) and good capacity for the inhibition of self- and Cu-mediated A β aggregation, with dependence on the linker size and substituent groups of each main moiety. Neuroprotective effects were also found for the compounds through viability assays of neuroblastoma cells, after A β _{1–42} induced toxicity. Structure-activity relationship analysis provides insights on the best structural parameters, to take in consideration for future studies in view of potential applications in AD therapy.

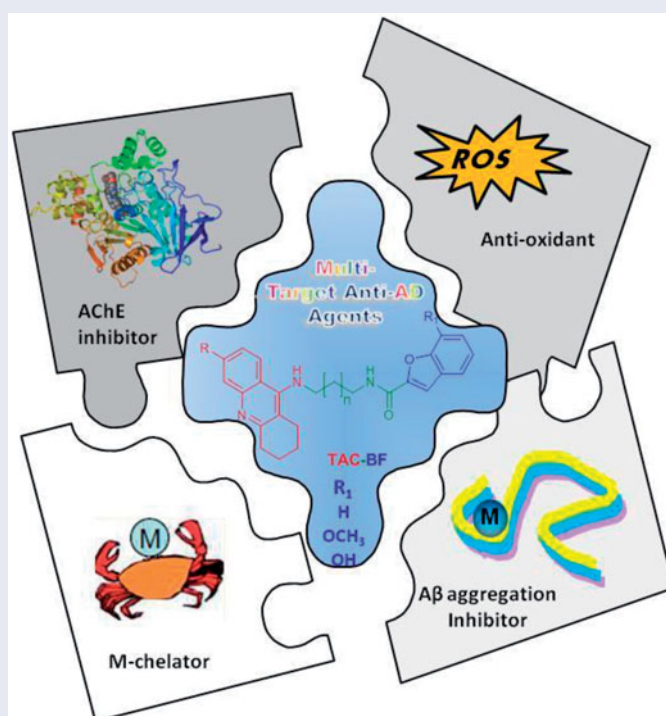
ARTICLE HISTORY

Received 27 August 2019
Revised 28 October 2019
Accepted 29 October 2019



KEYWORDS

Alzheimer’s disease; multi-target drugs; tacrine-benzofuran hybrids; AChE inhibitors; metal chelators

GRAPHICAL ABSTRACT



Design, synthesis and evaluation of new tacrine-benzofuran hybrids as multitargeting anti- Alzheimer’s disease agents; high AChE inhibition associated with other relevant properties; structure–activity relationship analysis

CONTACT M. Amélia Santos  masantos@tecnico.ulisboa.pt  Centro de Química Estrutural, Instituto Superior Técnico, Universidade de Lisboa, Av, Rovisco Pais 1, 1049-001, Lisboa, Portugal

*G.F. and K.C. contributed equally to this work.

© 2019 The Author(s). Published by Informa UK Limited, trading as Taylor & Francis Group.

This is an Open Access article distributed under the terms of the Creative Commons Attribution License (<http://creativecommons.org/licenses/by/4.0/>), which permits unrestricted use, distribution, and reproduction in any medium, provided the original work is properly cited.

1. Introduction

Alzheimer's Disease (AD) is one of the main causes of dementia among elderly people, whose prevalence by 2050 is expected to be 14 and 130 million people in Europe and worldwide, respectively^{1,2}. It is characterised by progressive impairment of memory cognitive functions due to the degeneration of synapses and to the death of neurons, especially in hippocampus³. The main pathological hallmarks of AD are the presence of thick extracellular β -amyloid plaques ($A\beta$) and intra-neuronal neurofibrillary tangles (NFT)⁴, which compromise brain function due to the death of many neurons. Other relevant characteristics of the patient brains are the deficit of choline neurotransmitters, mostly acetylcholine due to its hydrolysis by acetylcholinesterase (AChE) in neuronal synapses, and also the metal dyshomeostasis associated with advanced oxidative processes. In spite of the huge amount of research aimed at understanding and to combat this pathology, there is no cure so far. Along the past two decades, several strategies have been followed bringing important contributions to AD drug design and therapy⁵. The inhibition of AChE appeared as the first approach and four AChE inhibitor drugs (tacrine, donepezil, galantamine and rivastigmine) were approved by the US FDA, although they can only lead to temporary symptom amelioration⁶. Despite enormous efforts in the recent past years from academia and pharmaceutical companies, several new molecules failed on clinical trials⁷.

Due to the multifactorial nature of this disease, the perspective of AD treatment with a single-target molecule has been recently changed with the emergence of multi-target anti-AD drug candidates, aimed at targeting the disease pathogenesis and get disease-modifying effects. This type of compounds can act on several disease targets, such as amyloid beta peptide ($A\beta$) aggregation, inhibition of AChE, modulation of metal dyshomeostasis and inhibition of MAO involved in the production of reactive oxygen species (ROS)^{8–11}. Therefore, the world of hybrid molecules has been discovered and deepened, namely by repositioning and extra-functionalization of already approved drugs such as acetylcholinesterase inhibitors (AChEi). Tacrine (TAC) is the first single drug developed for AD treatment as AChE inhibitor. Although it was withdrawn from the market due to its hepatic toxicity at therapeutic doses, it has been, by far, the mostly used AChE inhibitory moiety in the development of multi-target anti-AD drugs^{11–13}.

Continuing our recent efforts to discover novel multi-target directed ligands (MTDLs) for the treatment of AD, especially based on templates of already known AChEi drugs^{14–16}, the current study is focused on a new set of tacrine-benzofuran (TAC-BF) hybrids, which have been developed and evaluated for their multiple properties as potential multi-target anti-AD agents. The naturally inspired benzofuran (BF) scaffold can be considered as a mimic of the indanone moiety of donepezil, and it has been recently applied in many natural-based compounds with important biological properties, even as anti-neurodegeneratives^{15,17–19}. Particularly in this study, the new hybrids were designed to decide on the most adequate spacer length between both main molecular units, with aid from molecular docking simulations. Afterwards, the selected compounds were synthesised and tested for their physico-chemical properties, as anti-oxidant and metal chelation capacity, and biological properties (AChE inhibition, anti- $A\beta$ aggregation); the effects of the compounds on cell viability and neuroprotection were also evaluated in neuroblastoma cells after $A\beta_{1-42}$ induced toxicity.

2. Results and Discussion

2.1. Molecular design

The study of the new multifunctional hybrid compounds (Figure 1) involved a preliminary molecular design approach. Therefore, two main molecular moieties were selected, namely tacrine (TAC) and benzofuran (BF), to guarantee the hitting of at least two main pathophysiological targets of AD. TAC could assure the AChE inhibition; BF was selected to mimic the indanone role in donepezil (DNP), enabling a bimodal enzyme interaction for AChE, and also to inhibit the self-aggregation of $A\beta$ peptide; the hydroxyl BF substituent (β -positioned to the oxygen atom of BF) can also endow the hybrids with metal (Fe, Cu) chelating capacity and concomitant extra anti-oxidant activity. Besides the selection of the main scaffolds and corresponding linkers, substituent groups were also introduced in each moiety, namely: at C6 of TAC, the chlorine atom, aimed at improving the AChE inhibitory capacity; at C7 of BF, the methoxyl and hydroxyl groups, with the goal of mimicking DNP indanone substituent groups as well as to provide metal chelation capacity, respectively. To achieve the bimodal interaction of the hybrids with AChE, through the binding to both the catalytic anionic site (CAS) and the peripheral anionic site (PAS), the size of the linker chain, connecting both main moieties, is of expected relevance. Based on our previous experience about TAC hybrids with dual-binding site¹⁶, alkyl linkers were selected with 3–4 methylene carbons ($n=1, 2$), meaning a total spacer length of 5–6 atoms. Therefore, to get some insight on the effects of these structural variations on the binding pattern and binding affinity between the ligand and the receptor, molecular docking simulation appears as an important tool.

The model structure for the active site of AChE was obtained from the RCSB Protein Data Bank (PDB, entry 1ODC)²⁰, particularly from the X-Ray structure of *Torpedo Californica* AChE (*TcAChE*) complexed with the inhibitor (*N*-4'-quinolyl-*N'*-9''-(1'',2'',3'',4''-tetrahydroacridinyl)-1,8-diaminooctane), hereinafter named as the original ligand, which has structural similarities with our hybrids. Notwithstanding some recognised differences between the respective inhibitor-enzyme complexes, reported for human acetylcholine esterase, hAChE, and also of the electric ray (*Torpedo californica*) homologue, *TcAChE*, both enzymes are fairly conservative in terms of the main aminoacid residues that coat the active site gorge²¹, and so the herein described modelling study was performed with *TcAChE*.

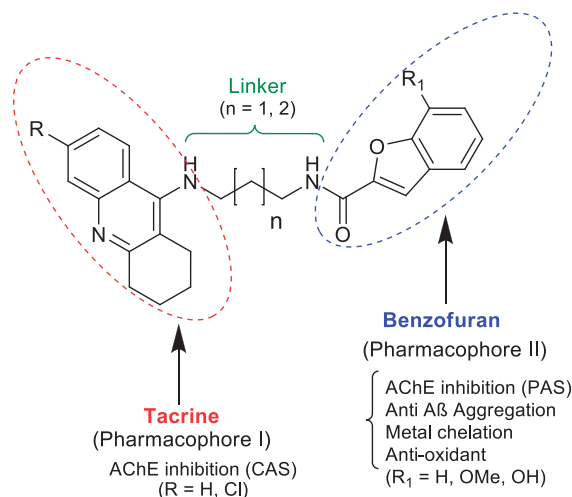


Figure 1. General structure of the tacrine-benzofuran (TAC-BF) hybrids under study.

Analysis of the outcomes of docking results (Figure 2) shows a perfect insertion of the TAC moiety into the CAS, lined with the residues Trp84, Phe330, Glu199, with a good superimposition of the TAC of the hybrids and that of the original ligand. This is mainly due to their ability to establish π - π stacking binding interactions with the aromatic rings of Trp84 and Phe330 (see Figure 2), which can block the entrance of the substrate (ACh) and therefore avoid its hydrolysis by the catalytic triad (Ser200, His440, Glu327)²². On the other hand, the BF moiety, linked to TAC by the alkylamide spacers, seems also to be able to establish π - π interactions with PAS through Tyr70 and Trp279 residues. Both the alkyl-amidic chain linkers of the conjugates, with three or four methylene groups ($n = 1, 2$) in the alkyl chains, appear to be well accommodated along the hydrophobic channel, providing the adequate lengths for dual mode interaction inside the AChE gorge and also H-bond interactions between the amide-NH and the phenolic group of Tyr121, in accordance with previously reported results for other TAC hybrids^{14,16}. Remarkably, the docking results show only small differences in the enzyme interaction with an apparent better interaction with shorter spacer (5 atoms in the tether chain; $n = 1$) than with the corresponding longer homologue (6 atoms in the tether chain; $n = 2$), (cf. **23** and **24**, Figure 2).

Regarding the effect of substituent groups, the chloro substitution at C6 of TAC is supposed to account for a better activity than the non-substituted analogues, due to the good fitting of the chlorine atom inside a hydrophobic pocket of TcAChE formed by Trp432, Met436 and Ile439²³, otherwise identically reported for the human AChE (hAChE)²⁴, although, in Figure 2, only the first residue (Trp432) can be seen in a close distance from the chlorine atom. Regarding the BF moiety, the C7 substitution by methoxyl/hydroxyl groups aimed at enabling eventual new potential interactions into the PAS. Indeed, it is interesting to observe that the BF moiety is well accommodated into the PAS, where -OCH₃/-OH seems to create H-bond interactions with the Tyr70, although the presence of the substituents may also cause a slight rearrangement of the whole structure inside this site, as compared with the non-substituted compounds. Overall, the molecular modelling studies gave some support to the predicted ability of the compounds for a bimodal interaction at CAS and PAS binding sites of AChE. Furthermore, BF is expected to bring other important contributions to the whole multifunctional activity of the studied hybrids (antioxidant activity, anti-A β aggregation and metal chelation), which will be object of study in the respective sections.

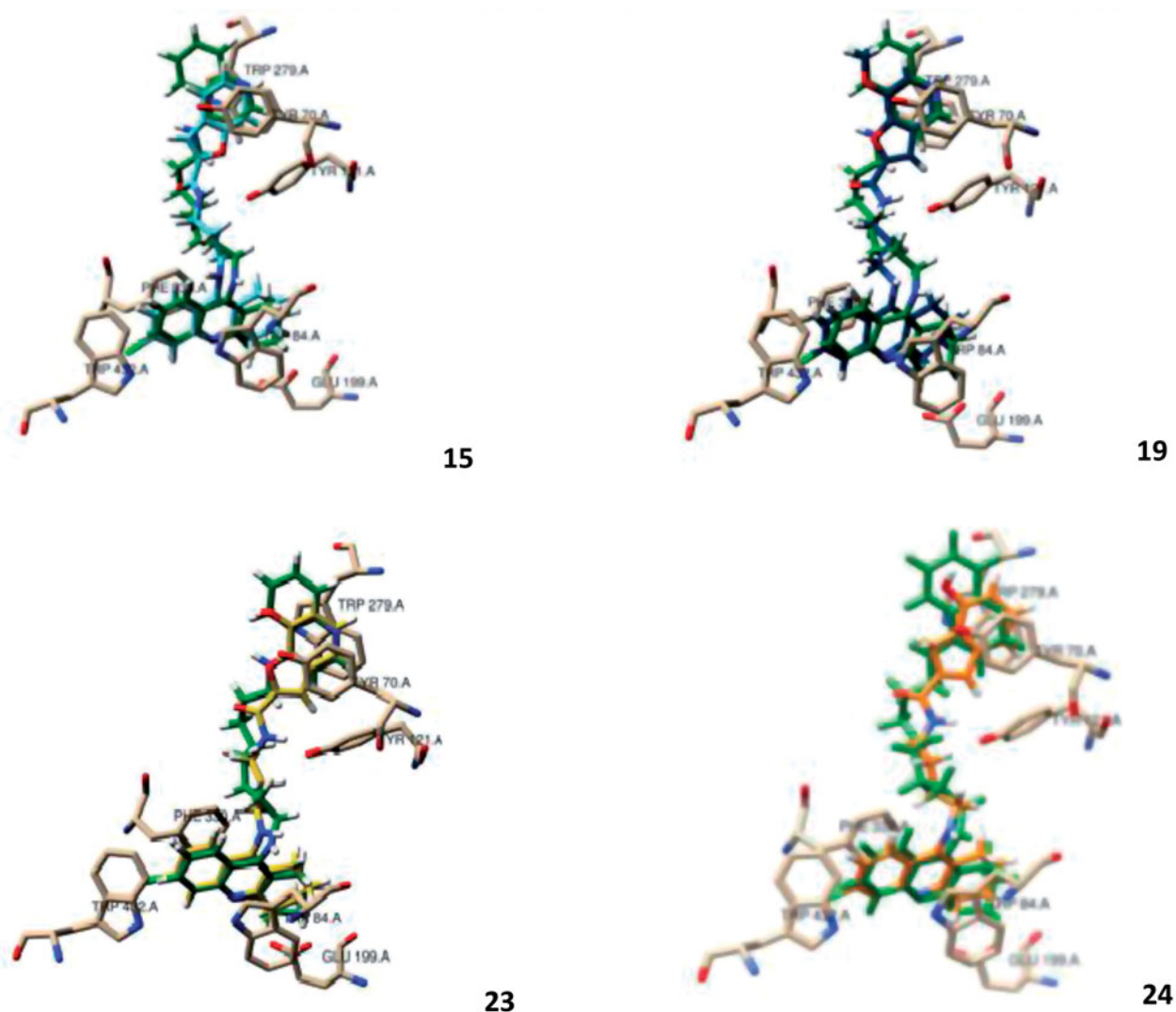


Figure 2. Molecular modelling of four representative compounds inside the binding site of AChE, superimposed with the original ligand (*N*-4'-quinolyl-*N'*-9''-(1'',2'',3'',4''-tetrahydroacridinyl)-1,8-diaminooctane), green Coloured. These compounds have the same TAC substituent ($R = \text{Cl}$), but different BF substituent (R_1) and spacer length: **15** (turquoise Coloured; $n = 1$; $R_1 = \text{H}$), **19** (dark blue Coloured; $n = 1$; $R_1 = -\text{OCH}_3$), **23** (yellow Coloured; $n = 1$; $R_1 = -\text{OH}$), **24** (orange Coloured; $n = 2$; $R_1 = \text{H}$).

It should be mentioned that after the design and synthesis of the herein studied series of hybrids, a publication appeared also with TAC-BF hybrids²⁵, although they have different linkers and do not include the same substituent groups, in particular the hydroxyl group of the benzofuran ring which is able to provide metal chelating capacity and additional anti-oxidant activity.

Comparison of the present docking simulations with those recently reported,²⁵ for two other Tacrine-benzofuran hybrid analogues, indicates quite identical interaction within the CAS binding site, although interaction with PAS at the entrance of the gorge involves different aminoacid residues, attributable to the difference in the used crystal structure of the inhibitor-bound TcAChE complexes and also to the much longer length of the linker for the two most closed analogues (from 3 to 6 carbon atom chain, in the present and the reported studies).

2.2. Chemistry

The series of eight TAC-BF hybrids was prepared by following the synthetic strategy outlined in Scheme 1. It involved two independent sequential reaction steps leading to the preparation of the two main molecular moieties (TAC and BF), which were then coupled to each other. The TAC starting fragments, 9-chloro-1,2,3,4-tetrahydroacridines (**3/4**), were prepared from the coupling of the commercially available anthranilic acid (**1**) or 2-amino-4-chlorobenzoic acid (**2**) with cyclohexanone in the presence of POCl₃, as previously reported²⁶. The synthesis of the BF derivatives involved a first condensation of the salicylaldehyde derivatives (**5/6**) (R₁ = H/OMe) with ethylbromoacetate in dry DMF under reflux and basic conditions for substitution at the phenol group to obtain the intermediate esters, ethyl 2-phenoxyacetates (**5'/6'**), which were subsequently cyclized by further heating at high temperature conditions to afford the corresponding intermediate BF-esters (**7/8**). Reaction of the diaminoalkane spacers with the benzofuran-2-ethylcarboxylates in methanol gave the corresponding *N*-(aminoalkyl)benzofuran-2-carboxamides (**9–12**). These aminoalkyl-benzofuran derivatives were finally attached at the 9-position of the TAC derivatives (**3/4**), by their reaction in the presence of phenol and a catalytic amount of potassium iodide, affording the final compounds (**13–20**). The methoxy-containing compounds (R₁ = -OCH₃, **18–20**) were further demethylated to obtain the corresponding derivatives with R₁ = -OH (**21–24**). This

reaction involved a standard acidic hydrolysis under very mild conditions, namely with a mixture of the Lewis acid boron trichloride (BCl₃) and the catalyst tetra-*n*-butylammonium iodide (TBAI), in dry CH₂Cl₂, under N₂ atmosphere and low temperature (−78 °C), following a protocol previously reported^{27,28}.

2.3. Physico-chemical studies

2.3.1. Radical scavenging activity

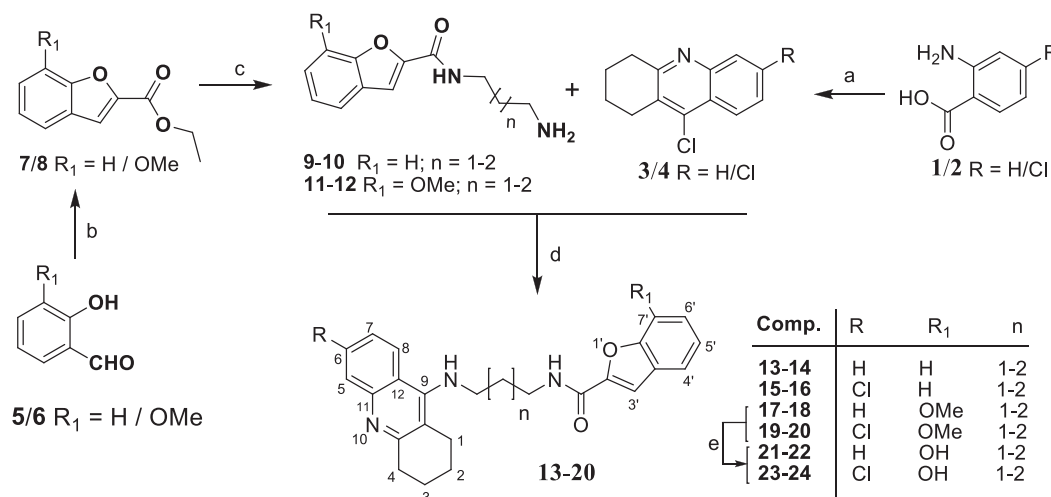
A selection of the newly synthesised hybrids was tested for their radical scavenging activity (anti-oxidant activity, EC₅₀), based on their interaction with the 2,2-diphenyl-1-picrylhydrazyl (DPPH) free radical, as previously described²⁹.

Analysis of the obtained results indicate for compound **20** a weak activity (EC₅₀ >10³ μM), otherwise similar to that found for the reference compound, TAC. However, the introduction of the hydroxyl substituent in the BF moiety resulted in a considerable increase of the radical scavenging activity, though with still moderate EC₅₀ values (434–480 μM, for **24** and **21**). Overall, the presence of the hydroxyl group increases the hybrid anti-oxidant activity, as previously anticipated, which can be attributed to their capacity for proton donation from the OH group.

2.3.2. Metal complexation

It has been largely accepted that chelators interfere both in metal-induced Aβ aggregation/neurotoxicity and on metal homeostasis of AD brains. Among the hybrids with BF hydroxyl substituent, compound **21** was chosen as a representative model to analyse the concomitant chelating capacity towards the redox-active (Fe(III), Cu(II)) and Aβ-binding (Cu(II)) metal ions. Due to solubility reasons, these studies were performed in a mixed 25% (w/w) DMSO/water medium. In fact, DMSO was chosen because it is a widely used and well tolerated solvent in biological and cellular studies, the amounts of ligand (<7 μM) and DMSO (<1%) employed in culture media being quite low with concomitant no alterations observed in cells³⁰.

The protonation constants of compound **21**, corresponding to the phenolic hydroxyl (log K₁ = 9.01) and to the tacrine *N*-amine (log K₂ = 7.99) groups, were determined by ultraviolet-visible (UV-vis) spectrophotometric titration (see Figure 3 and Table 1). Figure 3 shows that the absorbance maxima at 339 and 351 nm correspond



Scheme 1. Synthesis of TAC-BF hybrids. Reagents and conditions: (a) cyclohexanone, POCl₃, 180 °C, 3 h; (b) DMF, K₂CO₃ (1.2 eq), ethylbromoacetate (1.05 eq), 135–140 °C, 5–6 h; (c) diaminoalkane (3.0 eq), dry MeOH, overnight; (d) phenol, KI, 165–170 °C 35–60 min; (e) BCl₃, TBAI, DCM, under N₂ (−78 °C), 2 h.

to both species (H_2L^+ and HL), while those at 295 and 321 nm are attributed to the deprotonated (L^-) form.

From analysis of Table 1 it is possible to conclude that the obtained $\log K_i$ values are in accordance with the values found, in 50% w/w DMSO/water medium, for the protonation of the phenolic oxygen ($\log K_1 = 9.02$ and the tacrine *N*-amine ($\log K_2 = 8.18$) of TAC-BIM1³¹.

The chelating ability of compound **21** towards the two metal ions under study (Fe(III) and Cu(II)) was evaluated on the basis of

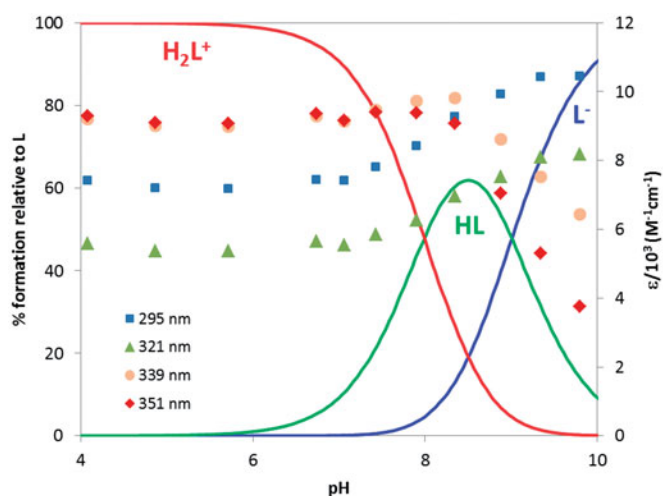
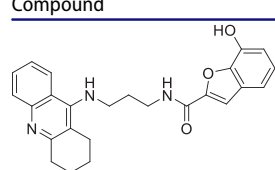
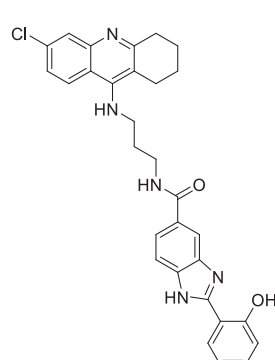


Figure 3. Species distribution curves for compound **21** along with molar extinction coefficients at the maximum absorption wavelengths ($C_L = 4.0 \times 10^{-5}$ M).

Table 1. Stepwise protonation constants for the ligand **21** and global formation constants^a for the corresponding Fe(III) and Cu(II) complexes ($T = 25.0 \pm 0.1$ °C, $I = 0.1$ M KCl, 25% w/w DMSO/water) as well as pM^b values.

Compound	$M_mH_nL_l$	$\log K_i$	$\log \beta_{Fe_mH_nL_l}$	$\log \beta_{Cu_mH_nL_l}$
 21	(011)	9.01(1)	–	10.87(6)
	(021)	7.99(3)	–	19.02(2)
	(101)	–	22.90(6)	20.68(8)
	(111)	–	38.37(6)	–
	(102)	–	36.95(7)	–
	(112)	–	–	–
	(103)	–	–	–
	(1–11)	–	–	2.25(3)
	(1–22)	–	12.21(8)	–
	pM			22.2
 TAC-BIM1^c	(011)	9.02(3)	–	17.27(5)
	(021)	8.18(5)	–	34.38(6)
	(031)	3.32(6)	–	20.14(8)
	(111)	–	–	–
	(122)	–	–	–
	(102)	–	–	–
	pM			

^a $\beta_{M_mH_nL_l} = [M_mH_nL_l]/[M]^m[H]^n[L]^l$.

^b $pM = -\log[M]$ at pH 7.4 ($C_L/C_M = 10$, $C_M = 1.0 \times 10^{-6}$ M).

^cIn 50/50 w/w DMSO/water³¹.

the global formation constants of the complexes, obtained by treatment of the UV-vis spectrophotometric data (see Table 1).

From Figure 4(a) it is possible to observe that, under the working conditions, $FeHL$ and $FeHL_2$ are the predominant species up to pH ca 8 and above that pH FeL_3 and $FeL_2(OH)_2$ are subsequently formed. Compound **21** is a strong chelator for iron ($pFe = 22.2$ at pH 7.4, $C_L/C_M = 10$, $C_M = 10^{-6}$ M), that can be attributed to the *hard* donor atom (*O,O*) chelation core of the BF moiety and the formation of stable five-membered metal chelate rings.

Concerning copper chelation, Figure 4(b) presents $CuHL$ as the dominant species below pH 6.7 while above it, CuL_2 is the predominant species. Compound **21** is a good copper chelator ($pCu = 11.9$), similarly to already found for the hydroxyphenyl-benzimidazole (BIM) derivatives ($pCu = 10.7$ – 11.1)³¹.

As a conclusion, the hydroxyl-containing derivatives of these TAC-BF compounds showed to be effective chelators of Fe(III) and Cu(II), well-known redox-active metal ions associated to AD.

2.4. Biological activity

2.4.1. AChE inhibition

Inhibition of *TcAChE* by the new set of hybrids (**13**–**24**) was evaluated by using a previously described method²⁹, based on an adaptation of the Ellman's test³². The standard reference compound selected for these assays was tacrine ($IC_{50} = 0.35$ μ M)¹⁴, which was also evaluated under our experimental conditions. The IC_{50} values obtained for AChE inhibition (AChEi) are depicted in Table 2. All the studied

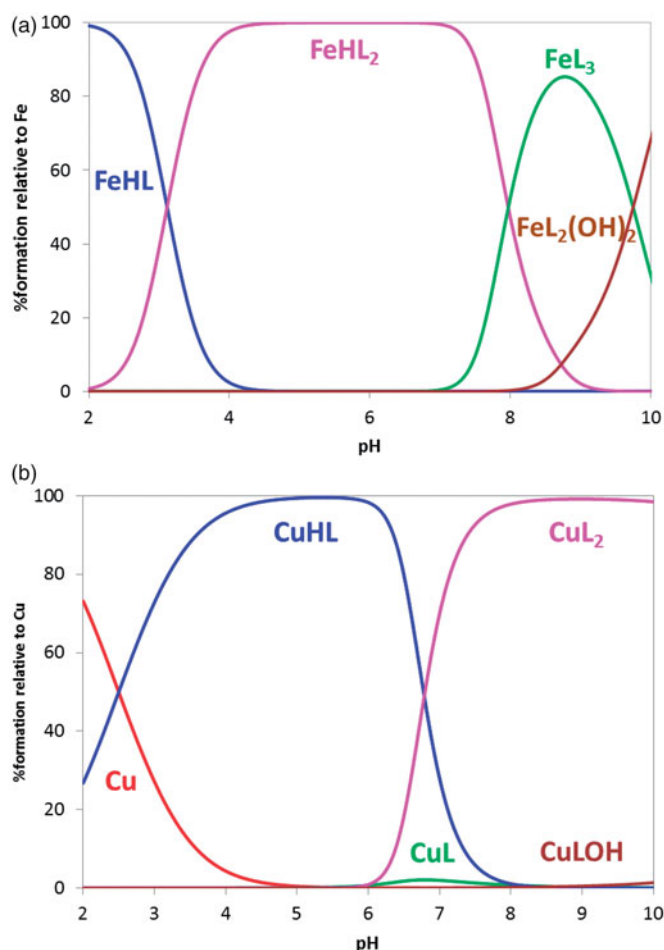


Figure 4. Species distribution curves for the systems (a) Fe(III)/**21** 1:3 and (b) Cu(II)/**21** 1:2 ($C_L = 4.0 \times 10^{-5}$ M).

compounds showed good inhibitory activity, with IC_{50} values in sub-micromolar range, close or even inferior to that of the standard reference. A brief structure-activity relationship analysis was performed, to aid the comparison and understanding of the contribution of different structural variations in the inhibitory activity, namely the length of the spacer, as well as the presence of substituent groups in tacrine (H, Cl) and in benzofuran (-H, -OCH₃, -OH), as illustrated on the graphics (A, B, C) of Figure 5.

Graph A illustrates the effect of the linker length on the enzyme inhibitory capacity. Remarkably, the compounds with propylic chains evidenced higher AChE inhibitory activity than the butylic analogues, although the molecular modelling only indicated a subtle better accommodation of the shorter length inhibitors inside the enzyme active site. The compounds with longer linker may be forced to some structural distortions, namely in their interactions inside the lipophilic channel between CAS and PAS and

Table 2. Summary of results for the biological assays of TAC-BF hybrids

Comp.	n	R	R ₁	AChE inhibition ^a IC_{50} (μ M)	$A\beta$ aggregation inhibition ^{b,c} (%)	
					Self- $A\beta$ aggr	Cu-ind $A\beta$ aggr
13	1	H	H	0.58	60.6	–
14	2	H	H	0.72	51.5	–
15	1	Cl	H	0.12	51.0	–
16	2	Cl	H	0.34	43.0	–
17	1	H	OCH ₃	0.36	57.5	–
18	2	H	OCH ₃	0.76	51.9	–
19	1	Cl	OCH ₃	0.13	57.8	–
20	2	Cl	OCH ₃	0.67	64.4	–
21	1	H	OH	0.81	44.0	50.1
22	2	H	OH	0.98	30.4	54.0
23	1	Cl	OH	0.13	31.5	52.5
24	2	Cl	OH	0.61	43.4	53.4
TAC	–	–	–	0.35	20	–

^aThe values are mean of five independent experiments \pm SD; AChE from *Electric eel*.

^bInhibition of self-mediated $A\beta_{42}$ aggregation (%) with or without copper (40 μ M). The thioflavin-T fluorescence method was used, and the measurements were carried out in the presence of an inhibitor (80 μ M).

^cThe values are the mean of two independent measurements in duplicate (SEM < 10%).

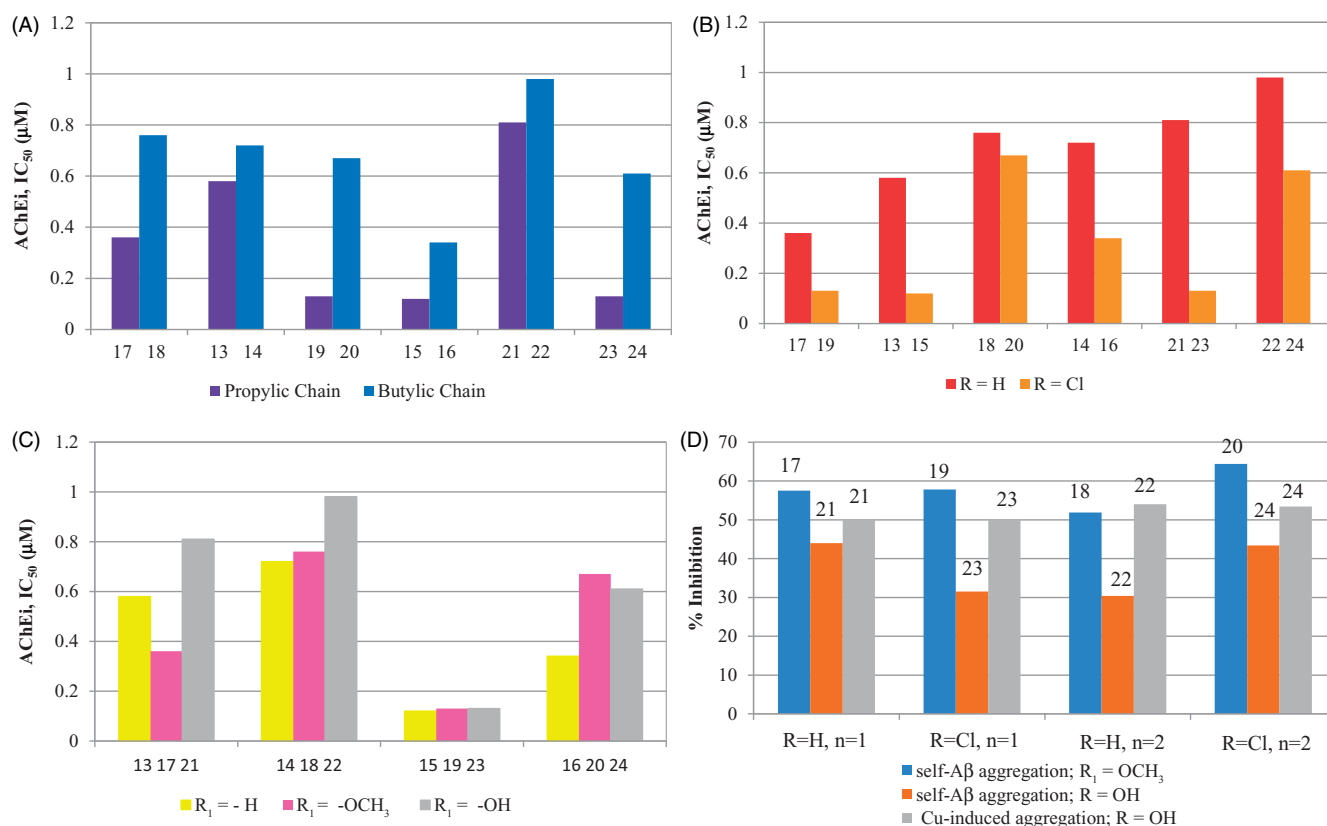


Figure 5. Graphical summary of the effect of different structural parameters on the inhibition of AChE (AChEi, IC_{50}) and on the inhibition of $A\beta$ aggregation (%): (A) size of alkylchain linker in AChEi: $n = 1$ (propylic chain), $n = 2$ (butylic chain); (B) substituents at C6 of TAC (R = H, Cl) in AChEi; (C) substituents at C7 of BF ($R_1 = H$, -OCH₃, -OH) in AChEi; (D) inhibition of $A\beta$ aggregation (self- and Cu-induced).

even in the stacking interaction of BF with PAS. Interestingly, identical chain length effects were also found in other tacrine hybrids¹⁶. Graph **B** illustrates the effect of chlorine substitution in TAC, which led to improvement of the inhibitory activity of the hybrids, consistently with other results previously described^{14,22}, although the major effect was shown for those with the propylic chain and OH substituent (cf. **21** and **23**). Graph **C** indicates that the BF substituents (-OCH₃ or -OH) do not lead to activity improvement. Overall, the best AChEi activity was achieved for hybrids **15**, **19** and **23** with propylic chain linkers and, except **19**, as well as chloro substitution on TAC and no substitution on the BF moiety.

Although not measured under the framework of this paper, the inhibition of butylcholinesterase (BuChE) and the selectivity of both cholinesterases could be also of interest to be pursued in future evaluations.

2.4.2. Inhibition of self- and Cu²⁺-induced A β ₁₋₄₂ aggregation

The A β amyloid plaques are one of the main hallmarks of AD and they result from over production and aggregation of β -amyloid peptide, which can accumulate outside the neurons, by self-mediated or Cu²⁺-induced process, interfering with the synaptic impairment, neurotransmission and memory³³. Therefore, anti-AD drugs have been designed aimed to disrupt and disaggregate the A β 's fibrils into monomers, obtaining non-toxic forms of β -secretase's products³⁴. To assess the effect of these new hybrids in the inhibition of amyloid peptide aggregation, a selection of the compounds was *in vitro* assayed, based on the thioflavin T (ThT) method³⁵. Indeed ThT is a histochemical dye able to create ionic or hydrophobic interactions with the peptide β -sheets, the predominant secondary structure of the amyloid fibrils in aqueous solutions³⁶. This binding interactions can be monitored by fluorimetry since the presence of ThT-fibrils increases the absorbance and the emission of the ThT dye, and induces red shifts on the absorbance (from 385 to 446 nm) and emission peaks (from 445 to 485 nm)¹⁴. All the measurements were performed after incubation of the self-mediated and Cu²⁺-induced A β aggregates in the presence/absence of the herein

studied compounds. The results, expressed as percentage of aggregation inhibition, are summarised in Table 2 and graphically presented in Figure 5(D), including the values obtained for Tacrine (20% of inhibition) as standard reference for comparison purpose. They showed that all compounds can inhibit the A β aggregation with good-to-moderate activity and improved as compared with TAC. Their activity and their dependence on ligand structural features may be rationalised by different intercalation into the fibrils, as already postulated and reported for other inhibitors^{14,37}. Among the compounds in study, **20** exhibited the highest inhibitory activity in both kinds of induced A β aggregation, while others (ex. **17**, **18**, **19**) present also very good activity for self-mediated A β aggregation, but they are expected to have moderate activity for Cu²⁺-induced A β aggregation due to absence of the OH group. Interestingly, the hydroxyl substituent (**21-24**) seems to lead to a general inhibitory activity decrease of the self-mediated A β aggregation (as compared with the non-substituted or the methoxy-substituted analogues), while the inhibitory capacity towards the Cu²⁺-induced A β aggregation increased, as compared with conditions of metal absence. This may be rationalised on the basis of their copper chelating capacity, as previously shown by other metal chelating compounds^{14,38}. Furthermore, despite some exceptions (e.g. **20** and **24**), the increase in linker length and the chloro TAC substitution induce some small negative effects in the inhibition of A β self-aggregation.

Nevertheless, since quantitative analysis based on fluorescence of copper(II) containing solutions may result in somehow erroneous conclusions due to some potential emission quenching by this paramagnetic ion, a fluorescence-independent study by transmission electron microscopy (TEM) was also performed for compound **21**. The TEM images depicted in Figure 6 show the presence of heavily intertwined aggregates, for A β ₄₂ alone, while in the case of its co-incubation with **21** the aggregates became sparser and more elongated, thus suggesting that for this TAC-BF hybrid the A β self-induced aggregation maybe be mainly attributed to the ligand intercalation between β -sheets of A β fibrils. The presence of copper induced changes in the morphology of the A β aggregates, both in the absence and in the presence of

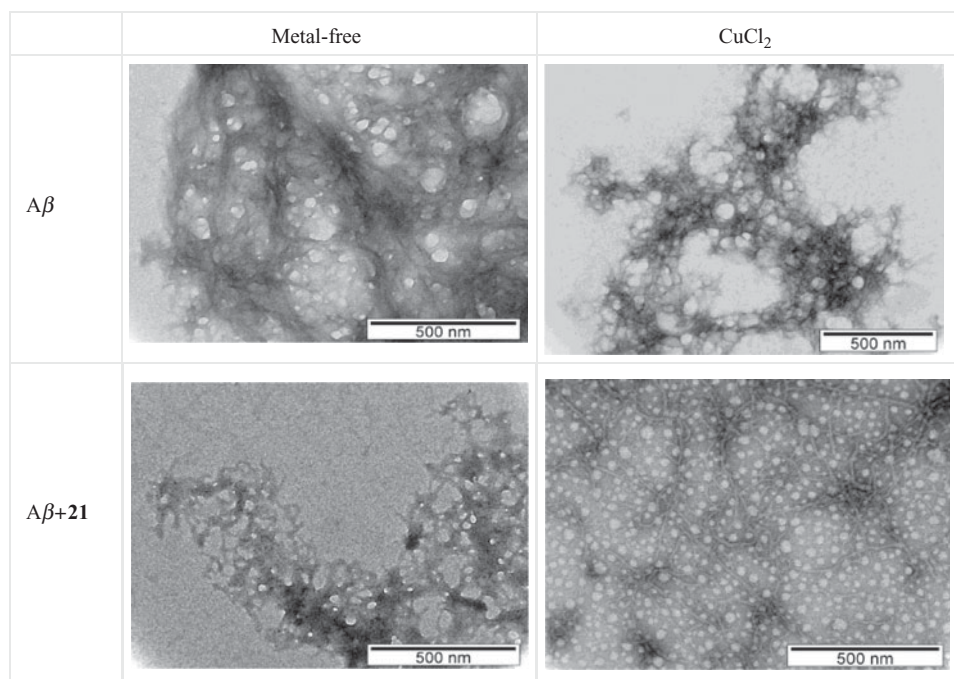


Figure 6. TEM images of A β aggregation inhibition performed with samples incubated (37 °C) for 24 h. Experimental conditions: [A β ₁₋₄₂] = [CuCl₂] = 25 μ M; [**21**] = 50 μ M; pH = 6.6.

21, although in this last case there is a considerable change, apparently with the formation of homogenous low molecular aggregates. Overall, TEM confirms the role of the ligand in the inhibition of A β aggregation.

2.4.3. Pharmacokinetic parameters

To assess the drug-likeness of these new drug candidates, some relevant pharmacokinetic parameters were *in silico* calculated to identify possible peripheral or central toxicity and to evaluate their ability to cross membranes, namely the blood-brain barrier (BBB), in case of drugs which main goal is the CNS. Thus, all the studied compounds have been evaluated by QikProp V. 2.5 program³⁹, to gain prediction on some pharmacokinetic parameters, such as: the lipophilic character, (the octanol–water partition coefficient, *clog P*), the capacity to cross the BBB (*log BB*), the velocity of intestinal absorption (caco-2 cell permeability), the activity in the CNS and also the verification of Lipinski's rule of five, to give an idea of potential future oral formulation as anti-AD agents (see Table 3).

Analysis of the results depicted in Table 3 shows that important parameters, such as molecular weight, *clog P* and *log BB*, are perfectly inside the range determined by Lipinski's rule to act in the CNS, though it has been noticed that one parameter has been violated except for **21**, **22** and **23**. In fact, most of the values

calculated for *clog P* are close to the limit imposed by the used range, warning for possible negative consequences on the absorption through the BBB due to their lipophilic components (presence of longer chain or absence of polar hydroxyl groups). Furthermore, all the compounds evidenced good capacity to cross the intestinal cell barrier for a good GUT absorption, though the last four compounds have lower values, apparently due to the presence of that hydrophilic group. Lastly, but not less important, the predicted CNS activity, related to toxicological effects, indicates they should be safe and without anticipated side effects.

2.4.4. Cell viability and neuroprotection

The neuroprotective effect of these new multi-target drugs designed for AD was evaluated using SH-SY5Y cells treated with A β_{1-42} peptides or ascorbate/iron. For each compound we performed a dose-response curve to select a non-toxic concentration (Figure 7).

AD is characterised by the extracellular accumulation of senile plaques composed of aggregated amyloid-beta peptide (A β). A β peptides are synthesised inside cells where they oligomerize and may react with active metal-ions such as copper, iron or zinc. The production of ROS conjugated with oligomeric A β peptide is involved in the neurodegenerative process of AD⁴⁰. We observed

Table 3. Summary of calculated pharmacokinetic molecular descriptors for the new hybrids by QikProp v.2.540³⁹

Comp. Ref.	(n,R,R1)	MW ^a	<i>clog P</i> ^b	<i>log BB</i> ^c	Caco-2 Permeability ^d (nm/sec)	Violations of Lipinski's rule of 5 ^e	CNS activity ^f
13	(1,H,H)	399.491	5.143	-0.690	1764	1	+/-
14	(2,H,H)	413.518	5.106	-0.488	2173	1	+/-
15	(1,Cl,H)	433.936	5.685	-0.396	2149	1	+/-
16	(2,Cl,H)	447.963	6.039	-0.559	1893	1	+/-
17	(1,H,OCH ₃)	429.518	5.327	-0.573	2423	1	+/-
18	(2,H,OCH ₃)	443.544	5.745	-0.802	1867	1	-
19	(1,Cl,OCH ₃)	463.963	5.852	-0.431	2324	1	+/-
20	(2,Cl,OCH ₃)	477.989	5.907	-0.597	1890	1	+/-
21	(1,H,OH)	415.491	4.567	-1.522	460	0	-
22	(2,Cl,OH)	429.518	4.755	-1.466	520	0	-
23	(1,Cl,OH)	449.936	4.764	-1.261	469	0	-
24	(2,Cl,OH)	463.963	5.208	-1.324	493	1	-

^aMW < 500.

^b-2 < *clog P* < -6.5.

^c-3.0 < *log BB* < 1.2.

^d<25 poor and >500 great.

^eMaximum is 4.

^f(-) inactive toxicologically - (++) very active toxicologically³⁹.

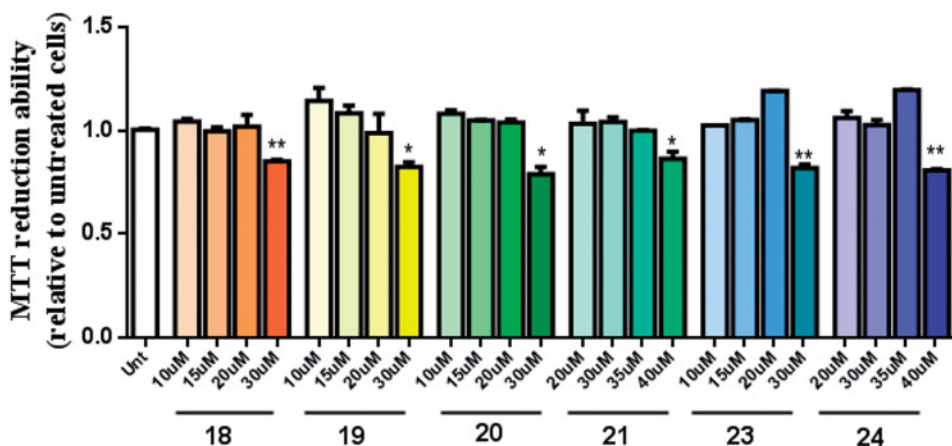


Figure 7. Dose-response screening to select non-toxic concentrations of TAC-BF hybrids. Cells were treated with varying concentration of TAC-BF conjugates (from 10 μ M to 40 μ M) for 25 h and cell viability was determined using the MTT reduction assay. Results are expressed relatively to SH-SY5Y untreated cells, with the mean \pm SEM derived from three different experiments. * p < 0.05; ** p < 0.01, significantly different when compared with SH-SY5Y untreated cells.

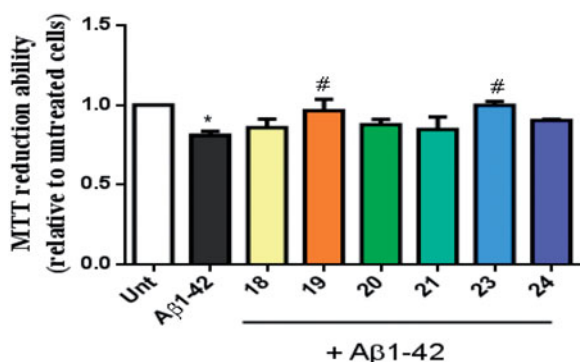


Figure 8. Neuroprotective effect of TAC-BF hybrids from Aβ₄₂-induced toxicity on SH-SY5Y cells. Cells were treated with Aβ₄₂ peptide (2.5 μM) for 24 h in the absence or in the presence of the compounds (1 h pre-incubation + 24 h co-incubation). Evaluation of cell viability was performed using the MTT reduction assay. Results are expressed relatively to SH-SY5Y untreated cells, with the mean ± SEM derived from 4 different experiments. **p* < 0.05, significantly different when compared with SH-SY5Y untreated cells; #*p* < 0.05, significantly different when compared with Aβ₄₂ treated SH-SY5Y cells. (compounds: **18**, **19**, **20** and **23** – 20 μM; **21**, **24** – 35 μM).

that Aβ₄₂ decreased cellular viability and, interestingly, the TAC–BF conjugates **19** and **23** prevented that Aβ-induced cell toxicity (Figure 8).

Compound **19** showed ability to inhibit Aβ-self-aggregation, thus being expected to decrease the formation of oligomers and ROS-dependent production. In addition, oxidative stress is an early event in the course of AD neurodegenerative process and it is associated with increased oxidation of proteins, lipids and nucleic acids in AD hippocampus and cortex. These data correlates with the elevated levels of Aβ₄₀ and Aβ₄₂ in the same brain regions⁴⁰. To induce oxidative stress in our cellular model we used the pair Asc/Fe, which showed a decrease in the viability of SHSY-5Y cells (Figure 9). Nevertheless, among the new TAC-BF hybrids tested, compound **19** appeared to best achieve cell protection from Asc/Fe-Induce oxidative stress, thus presenting the best radical scavenging properties in cell environment. Therefore, although in solution conditions the hydroxyl-containing compounds (**21–24**) revealed higher radical scavenging capacity than the tested non-hydroxyl compound (**20**), that feature was not paralleled in cell environment. This may be due to the higher hydrophilic character of these compounds (see Table 3). In fact, compound **21** evidenced the worst values calculated for BBB and Caco permeability and presented also the lowest capacity for in cell radical scavenging.

3. Conclusion

A new set of tacrine-benzofuran hybrids was designed, synthesised and studied through a multidisciplinary approach. These new compounds evidenced very good capacity for inhibition of AChE (submicromolar range), with the best activity found for compounds **15**, **19**, **23**, with IC₅₀ values much lower than that of tacrine (TAC). Therefore, according to the design aims, the extra-functional benzofuran (BF) moiety enabled the hybrids with dual-binding capacity in their interaction with the active binding sites (CAS and PAS) of the enzyme. Structure activity relationships, indicate that the best activity corresponds to compounds with a shorter linker (propyl chain) and chloride substituent at C6 position of TAC; the substituents at the C7 of BF did not evidence considerably systematic effects in the inhibitory activity, but the –OH causes a general small decrease. Regarding the inhibition of Aβ aggregation, the activity seems to be mainly related to the

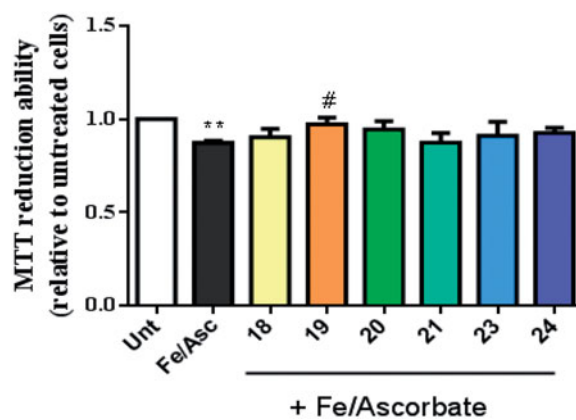


Figure 9. Neuroprotective effect of TAC-BF conjugates against L-Ascorbic Acid (AscH(-))/Ferrous Sulphate (Fe) toxicity on SH-SY5Y cells. Cells were treated with Asc/Fe (5 mM/500 μM, respectively) for 24 h, after treatment for 1 h in the absence or in the presence of the compounds. Evaluation of cell viability was performed by using MTT reduction assay. Results are expressed relatively to SH-SY5Y untreated cells, with the mean ± SEM derived from 4 different experiments. ***p* < 0.01, significantly different when compared with SH-SY5Y untreated cells. #*p* < 0.05, significantly different when compared with Asc/Fe treated SH-SY5Y cells. (compounds: **18**, **19**, **20** and **23** – 20 μM; **21**, **24** – 35 μM).

intercalating ability of the compound inside the fibrils. The best capacity for inhibition of Aβ self-aggregation was presented by **20** followed by compounds **17**, **18**, **19**. The OH-containing compounds present a general decrease in the self-aggregation inhibition although, in the presence of Cu²⁺, the inhibition is generally increased attributed to metal chelating effect. Furthermore compounds **19** and **23** presented the best achievements in terms of cell neuroprotective effects. Overall, a set of TAC-BF hybrids presented very good properties for potential drugs against AD and they deserve to be further explored for the challenging discovery of new AD therapies.

4. Experimental part

4.1. Materials and equipment

Analytical grade reagents were purchased from Sigma-Aldrich and Acros, and were used as supplied. Solvents were dried according to standard methods⁴¹. The chemical reactions were monitored by Thin Layer Chromatography (TLC) using alumina plates coated with silica gel 60 F254 (Macherey-Nagel). Column chromatography purifications were performed on silica gel (Merck 230–400 mesh (Geduran Si 60)). The melting points (mp) were measured with a Leica Galen III hot stage apparatus and are uncorrected. The Proton and Carbon-13 NMR were recorded either on Bruker AVANCE III-300 (300 MHz and 75.5 MHz) or Bruker AVANCE III-400 (400 MHz and 100.5 MHz) NMR spectrometers, at 25 °C. Chemical shifts (δ) are reported in ppm from the standard internal reference tetramethylsilane (TMS) and the coupling constant values (*J*) are determined in Hertz. In ¹H NMR description, the following abbreviations are used: s = singlet, d = doublet, t = triplet, m = multiplet, dt = double triplet, dd = double doublet, td = triple doublet, bs = broad singlet, bd = broad doublet. Mass spectra (ESI-MS) were performed on a 500 MS LC Ion Trap mass spectrometer (Varian Inc., Palo Alto, CA, USA) equipped with an ESI ion source, operated in the positive ion mode. High-resolution mass spectra (HRMS) were obtained on a Bruker Impact II quadrupole mass spectrometer (Bruker Daltonics).

For the metal complexation studies, the aqueous iron (FeCl₃, 0.0177 M) and copper (CuCl₂, 0.015 M) stock solutions were

prepared from 1000 ppm standards (Titrisol) and their metal content was evaluated by atomic absorption. To prevent hydrolysis, the iron stock solution was prepared in excess of acid chloride and its exact concentration in HCl determined by the usual standard-addition method using 0.1 M HCl (Titrisol). The 0.1 M HCl solution, used in spectrophotometric titrations, was prepared from a Titrisol ampoule while the titrant was from carbonate free commercial concentrate (Titrisol, KOH 0.1 M ampoules). The KOH solution was standardised by titration with a solution of potassium hydrogen phthalate and was discarded whenever the percentage of carbonate, determined by Gran's method⁴², was greater than 0.5% of the total amount of base.

The electronic spectra and the AChE inhibition assays were performed in a 1-cm path length quartz cell with a Perkin Elmer Lambda 35 spectrophotometer equipped with a temperature programmer PTP1 + 1 Peltier System ($T = 25.0 \pm 0.1^\circ\text{C}$). The enzyme AChE 500 U, extracted from *Electrophorus electricus* (electric eel), was purchased from Sigma-Aldrich.

For the study of the β -amyloid ($A\beta$) aggregation, the ThT fluorescence assay was performed using a Varian Cary Eclipse fluorimeter at the following wavelengths: excitation (446 nm) and emission (485 nm). Amyloid β -peptide (1–42), $A\beta_{1-42}$, was purchased from GeneCust as a lyophilised powder stored at -20°C . TEM assays were performed with a Hitachi H8100 transmission electron microscope with a LaB6 filament (200 kV, 10000–20000 \times magnification) at MicroLab/IST.

4.2. Synthesis of the compounds

The schematic representation and the synthetic steps involved in the preparation of all TAC-BF hybrids and their intermediates are shown in Scheme 1.

4.2.1. General procedure for synthesis of 9-chloro-1,2,3,4-tetrahydroacridine (3–4)

The title compounds, 9-chloro-1,2,3,4-tetrahydroacridine (**3**) and 6,9-dichloro-1,2,3,4-tetrahydroacridine (**4**), were prepared from commercially available anthranilic acids according to our previous reported procedure^{14,16}.

4.2.2. General procedure for synthesis of ethyl benzofuran-2-carboxylate (7–8)

To a solution of substituted salicylaldehydes (72 mmol) and potassium carbonate (10 g, 72 mmol) in DMF (100 mL) was added ethylbromoacetate (12 g, 72 mmol). The reaction was refluxed in oil bath for 12 h and after completion of reaction, it was poured in cold water and the product was extracted with ethyl acetate¹⁹. The crude product was purified by column chromatography using 1% ethyl acetate-petroleum ether as eluent to yield the desired product (70–75%).

4.2.3. Ethyl benzofuran-2-carboxylate (7)

Yield 70%, mp $48 - 50^\circ\text{C}$; $^1\text{H NMR}$ (CDCl_3 , 300 MHz) δ : 7.69 (d, 1H, $J = 2.0$ & 7.8 Hz, H-4), 7.60 (d, 1H, $J = 8.4$ Hz, H-7), 7.54 (s, 1H, H-3), 7.43–7.48 (m, 1H, H-6), 7.26–7.33 (m, 1H, H-5), 4.45 (q, 2H, $J = 7.2$ Hz, CH_2CH_3), 1.44 (t, 3H, $J = 6.9$ Hz, CH_3CH_2); $^{13}\text{C NMR}$ (CDCl_3 , 100 MHz) δ : 159.59, 155.67, 145.69, 127.53, 126.94, 123.73, 122.76, 113.76, 112.35, 61.50, 14.32; m/z (ESI-MS): 190.54 $[\text{M}]^+$.

4.2.4. Ethyl 7-methoxybenzofuran-2-carboxylate (8)

Yield 75%, mp $56 - 57^\circ\text{C}$; $^1\text{H NMR}$ (CDCl_3 , 300 MHz) δ : 7.51 (s, 1H, H-3), 7.18–7.25 (m, 2H, H-4 and H-5), 7.10 (d, 1H, $J = 7.8$ Hz, H-6), 4.34 (q, 2H, $J = 7.2$ Hz, CH_2CH_3), 3.94 (s, 3H, OCH_3), 1.32 (t, 3H, $J = 7.2$ Hz, CH_3CH_2); $^{13}\text{C NMR}$ (CDCl_3 , 100 MHz) δ : 159.34, 145.95, 145.93, 145.35, 128.57, 124.37, 114.52, 114.00, 108.86, 61.38, 56.00, 14.30; m/z (ESI-MS): 243.08 $[\text{M} + \text{Na}]^+$.

4.2.5. General procedure for synthesis of *N*-(aminoalkyl)benzofuran-2-carboxamide (9–12)

To the mixture of diaminoalkane (4 eq) in methanol, 1 M solution of ethyl benzofuran-2-carboxylate (**7**, **8**) in methanol was added dropwise over a period of 5 h at room temperature. The reaction mixture was stirred overnight and completion of reaction was monitored on TLC. On completion, the reaction mixture was concentrated under reduced pressure and the residue so obtained was diluted 4 M HCl solution (100 mL) under ice cold condition and washed with DCM (3×25 mL). Finally the aqueous layer was basified with saturated sodium hydroxide solution to 11–12 pH, extracted with ethyl acetate and dried on sodium sulphate. The evaporation of ethyl acetate under reduced pressure gave the desired pure *N*-(aminoalkyl)benzofuran-2-carboxamides (**9–12**) as light yellow solids in 64–71% yield.

4.2.6. *N*-(3-aminopropyl)benzofuran-2-carboxamide (9)

The title compound was synthesised from reaction of compound **8** with 1,3-diaminopropane. Yield 64%; mp $120 - 121^\circ\text{C}$. $^1\text{H NMR}$ (400 MHz, $\text{MeOD}-d_4$) δ : 7.64 (d, 1H, $J = 8.0$ Hz, H-4), 7.52 (d, 1H, $J = 8.0$ Hz, H-7), 7.44 (s, 1H, H-3), 7.39 (t, 1H, $J = 8.0$ Hz, H-6), 7.25 (t, 1H, $J = 8.0$ Hz, H-5), 3.48 (t, 2H, $J = 8.0$ Hz, CH_2NHCO), 2.72 (t, 2H, $J = 8.0$ Hz, CH_2NH_2), 1.75–1.82 (m, 2H, $\text{CH}_2\text{CH}_2\text{CH}_2$); $^{13}\text{CNMR}$ (100 MHz, $\text{MeOD}-d_4$) δ : 159.89, 154.93, 148.67, 127.39, 126.74, 123.47, 122.34, 111.38, 109.76, 38.42, 36.39, 32.09; m/z (ESI-MS): 219.26 $[\text{M} + \text{H}]^+$.

4.2.7. *N*-(4-aminobutyl)benzofuran-2-carboxamide (10)

The title compound was synthesised from reaction of compound **8** with 1,4-diaminobutane. Yield 69%; mp $94 - 95^\circ\text{C}$. $^1\text{H NMR}$ (400 MHz, $\text{MeOD}-d_4$) δ : 7.70 (d, 1H, $J = 8.0$ Hz, H-4), 7.57 (d, 1H, $J = 8.0$ Hz, H-7), 7.42–7.47 (m, 2H, H-3 & H-6), 7.30 (t, 1H, $J = 8.0$ Hz, H-5), 3.44 (t, 2H, $J = 8.0$ Hz, CH_2NHCO), 2.73 (t, 2H, $J = 8.0$ Hz, CH_2NH_2), 1.55–1.71 (m, 4H, $\text{CH}_2\text{CH}_2\text{CH}_2\text{CH}_2$); $^{13}\text{CNMR}$ (100 MHz, $\text{MeOD}-d_4$) δ : 159.81, 154.98, 148.74, 127.42, 126.73, 123.48, 122.33, 111.36, 109.70, 40.52, 38.71, 28.92, 26.48; m/z (ESI-MS): 233.37 $[\text{M} + \text{H}]^+$.

4.2.8. *N*-(3-aminopropyl)-7-methoxybenzofuran-2-carboxamide (11)

The title compound was synthesised from reaction of compound **8** with 1,3-diaminopropane. Yield 66%; mp $116 - 117^\circ\text{C}$. $^1\text{H NMR}$ (400 MHz, $\text{MeOD}-d_4$) δ : 7.43 (s, 1H, H-3), 7.17–7.24 (m, 2H, H-4 & H-5), 6.96 (d, 1H, $J = 8.0$ Hz, H-6), 3.98 (s, 1H, OCH_3), 3.50 (t, 2H, $J = 8.0$ Hz, CH_2NHCO), 2.75 (t, 2H, $J = 8.0$ Hz, CH_2NH_2), 1.77–1.84 (m, 2H, $\text{CH}_2\text{CH}_2\text{CH}_2$); $^{13}\text{CNMR}$ (100 MHz, $\text{MeOD}-d_4$) δ : 159.82, 148.60, 145.66, 144.40, 128.93, 124.24, 114.09, 110.06, 108.33, 55.10, 38.34, 36.33, 31.96; m/z (ESI-MS): 249.45 $[\text{M} + \text{H}]^+$.

4.2.9. *N*-(4-aminobutyl)-7-methoxybenzofuran-2-carboxamide (12)

The title compound was synthesised from reaction of compound **8** with 1,4-diaminobutane. Yield 71%; mp $89 - 90^\circ\text{C}$. $^1\text{H NMR}$

(400 MHz, MeOD- d_4) δ : 7.44 (s, 1H, H-3), 7.18 – 7.25 (m, 2H, H-4 & H-5), 6.97 (d, 1H, $J=8.0$ Hz, H-6), 3.98 (s, 1H, OCH₃), 3.43 (t, 2H, $J=8.0$ Hz, CH₂NHCO), 2.70 (t, 2H, $J=8.0$ Hz, CH₂NH₂), 1.54–1.69 (m, 2H, CH₂CH₂CH₂CH₂); ¹³CNMR (100 MHz, MeOD- d_4) δ : 159.68, 148.70, 145.66, 144.39, 128.95, 124.26, 114.11, 110.03, 108.32, 55.12, 40.75, 38.82, 29.50, 26.51; m/z (ESI-MS): 263.44 [M + H]⁺.

4.2.10. General procedure for the synthesis of *N*-(4-((1,2,3,4-tetrahydroacridin-9-yl)amino)alkyl)benzofuran-2-carboxamide derivatives (13 – 20)

The mixture of 9-chloro-1,2,3,4-tetrahydroacridine (**3**, **4**) (1 eq) and *N*-(aminoalkyl)benzofuran-2-carboxamide (**9** – **12**) (1 eq) was heated in phenol (0.5 eq) with the catalytic amount of potassium iodide at 155 – 160 °C for 35 – 60 min. The completion of reaction was monitored on TLC. On completion, the dense oily reaction mixture was sonicated with ethyl acetate. The precipitates so obtained were filtered and washed with water and hexane to give light yellow coloured *N*-(4-((1,2,3,4-tetrahydroacridin-9-yl)amino)butyl)benzofuran-2-carboxamide derivatives (**13**–**20**); the compounds were purified either through crystallisation in ethylacetate-hexane or through column chromatography over silica (0.5 – 1.0% MeOH-DCM) in 67 – 79% yield.

4.2.11. *N*-(3-((1,2,3,4-tetrahydroacridin-9-yl)amino)propyl)benzofuran-2-carboxamide (13)

The title compound was synthesised from reaction of compounds **3** and **9**. Yield 67%; mp 145 – 146 °C. ¹H NMR (400 MHz, MeOD- d_4) δ : 8.39 (d, 1H, $J=8.0$ Hz, H-8), 7.71 – 7.77 (m, 3H, H-5, H-6 & H-4'), 7.48–.57 (m, 3H, H-7, H-7' & H-6''), 7.42 (s, 1H, H-3'), 7.34 – 7.36 (m, 1H, H-5'), 4.09 (brs, 2H, CH₂NH), 3.59 (brs, 2H, CH₂NHCO), 2.94 (brs, 2H, H-4), 2.75 (brs, 2H, H-1), 2.17 (brs, 2H, CH₂CH₂CH₂), 1.92 (brs, 4H, H-2 & H-3); ¹³CNMR (100 MHz, MeOD- d_4) δ : 160.16, 156.69, 154.98, 150.31, 148.32, 138.33, 132.55, 127.32, 126.94, 124.89, 123.60, 122.39, 118.64, 115.66, 111.63, 111.37, 109.92, 44.98, 36.05, 29.94, 27.87, 23.55, 21.54, 20.34; HRMS (ESI) calcd for C₂₅H₂₆N₃O₂ [M + H]⁺, m/z 400.2020, found 400.2034.

4.2.12. *N*-(4-((1,2,3,4-tetrahydroacridin-9-yl)amino)butyl)benzofuran-2-carboxamide (14)

The title compound was synthesised from reaction of compounds **3** and **10**. Yield 72%; mp 117 – 118 °C. ¹H NMR (400 MHz, MeOD- d_4) δ : 8.30 (d, 1H, $J=8.0$ Hz, H-8), 7.69 (t, 1H, $J=8.0$ Hz, H-6), 7.60 – 7.63 (m, 2H, H-5 & H-4'), 7.45 – 7.49 (m, 2H, H-7 & H-7'), 7.39 (t, 1H, $J=8.0$ Hz, H-6'), 7.32 (s, 1H, H-3'), 7.25 (t, 1H, $J=8.0$ Hz, H-5'), 3.96 (t, 2H, $J=8.0$ Hz, CH₂NH), 3.42 (t, 2H, $J=8.0$ Hz, CH₂NHCO), 2.89 (brs, 2H, H-4), 2.62 (brs, 2H, H-1), 1.87 (brs, 6H, H-2, H-3 & NHCH₂CH₂) 1.73 – 1.77 (m, 2H, CH₂CH₂CONH); ¹³CNMR (100 MHz, MeOD- d_4) δ : 159.73, 156.28, 154.86, 150.30, 148.52, 138.37, 132.43, 127.29, 126.79, 125.00, 124.88, 123.52, 122.30, 118.79, 115.72, 111.60, 111.34, 109.65, 38.48, 27.98, 27.42, 25.99, 23.47, 21.57, 20.40; HRMS (ESI) calcd for C₂₆H₂₈N₃O₂ [M + H]⁺, m/z 414.2176, found 414.2147.

4.2.13. *N*-(3-((6-chloro-1,2,3,4-tetrahydroacridin-9-yl)amino)propyl)benzofuran-2-carboxamide (15)

The title compound was synthesised from reaction of compounds **4** and **9**. Yield 73%; mp 124 – 125 °C. ¹H NMR (400 MHz, MeOD- d_4) δ : 8.17 (d, 1H, $J=8.0$ Hz, H-8), 7.67 (d, 1H, $J=8.0$ Hz, H-4'), 7.60 (s, 1H, H-5) 7.52 (d, 1H, $J=8.0$ Hz, H-7'), 7.43 (t, 1H, $J=8.0$ Hz, H-

6'), 7.39 (s, 1H, H-3'), 7.27 – 7.32 (m, 2H, H-5' & H-7), 3.86 (t, 2H, $J=8.0$ Hz, CH₂NH), 3.55 (t, 2H, $J=8.0$ Hz, CH₂NHCO), 2.87 (brs, 2H, H-4), 2.66 (brs, 2H, H-1), 2.06–2.09 (m, 2H, CH₂CH₂CH₂) 1.85–1.86 (m, 4H, H-2, H-3); ¹³CNMR (100 MHz, MeOD- d_4) δ : 160.07, 154.90, 154.61, 153.49, 148.32, 141.69, 136.88, 127.26, 126.91, 126.24, 124.68, 123.56, 122.36, 120.28, 115.27, 113.20, 111.34, 109.89, 45.05, 36.15, 30.08, 29.61, 23.89, 21.78, 20.87; HRMS (ESI) calcd for C₂₅H₂₅ClN₃O₂ [M + H]⁺, m/z 434.6482, found 434.6449.

4.2.14. *N*-(4-((6-chloro-1,2,3,4-tetrahydroacridin-9-yl)amino)butyl)benzofuran-2-carboxamide (16)

The title compound was synthesised from reaction of compounds **4** and **10**. Yield 70%; mp 127 – 129 °C. ¹H NMR (400 MHz, MeOD- d_4) δ : 8.32 (d, 1H, $J=8.0$ Hz, H-8), 7.72 (d, 1H, $J=8.0$ Hz, H-4'), 7.60 (s, 1H, H-5) 7.53 (d, 1H, $J=8.0$ Hz, H-7'), 7.45 – 7.49 (m, 2H, H-6' & H-7), 7.39 (s, 1H, H-3'), 7.34 (t, 1H, $J=8.0$ Hz, H-5'), 3.95 (t, 2H, $J=8.0$ Hz, CH₂NH), 3.45 (t, 2H, $J=8.0$ Hz, CH₂NHCO), 2.93 (brs, 2H, H-4), 2.69 (brs, 2H, H-1), 1.90–1.93 (m, 6H, H-2, H-3 & NHCH₂CH₂) 1.77–1.81 (m, 2H, CH₂CH₂CONH); ¹³CNMR (100 MHz, MeOD- d_4) δ : 159.75, 155.41, 154.91, 152.37, 148.52, 140.66, 137.71, 127.32, 126.84, 125.03, 123.56, 122.35, 119.21, 114.92, 112.88, 111.31, 109.67, 38.47, 28.93, 27.32, 25.87, 23.52, 21.66, 20.67; HRMS (ESI) calcd for C₂₆H₂₇ClN₃O₂ [M + H]⁺, m/z 448.6636, found 448.6677.

4.2.15. 7-Methoxy-*N*-(3-((1,2,3,4-tetrahydroacridin-9-yl)amino)propyl)benzofuran-2-carboxamide (17)

The title compound was synthesised from the reaction of compounds **3** and **11**. Yield 75%; mp 137 – 138 °C. ¹H NMR (400 MHz, MeOD- d_4) δ : 8.28 (d, 1H, $J=8.0$ Hz, H-8), 7.62 – 7.70 (m, 2H, H-5 & H-6), 7.45 (t, 1H, $J=8.0$ Hz, H-7), 7.33 (s, 1H, H-3') 7.19 – 7.20 (m, 2H, H-4' & H-5'), 6.96 – 6.97 (m, 1H, H-6'), 3.98 (t, 2H, $J=8.0$ Hz, CH₂NH), 3.94 (s, 3H, OCH₃), 3.52–3.53 (m, 2H, CH₂NHCO), 2.85 (brs, 2H, H-4), 2.66 (brs, 2H, H-1), 2.08–2.13 (m, 2H, NHCH₂CH₂) 1.84 (brs, 4H, H-2 & H-3); ¹³C NMR (100 MHz, MeOD- d_4) δ : 159.98, 156.02, 150.85, 148.32, 145.67, 144.40, 138.99, 132.08, 128.84, 124.72, 124.37, 119.34, 115.94, 114.08, 111.84, 110.17, 108.43, 55.07, 45.00, 36.15, 29.95, 28.27, 23.64, 21.60, 20.47; HRMS (ESI) calcd for C₂₆H₂₈N₃O₃ [M + H]⁺, m/z 430.2135, found 430.2142.

4.2.16. 7-Methoxy-*N*-(4-((1,2,3,4-tetrahydroacridin-9-yl)amino)butyl)benzofuran-2-carboxamide (18)

The title compound was synthesised from the reaction compounds **3** and **12**. Yield 79%; mp 111 – 113 °C. ¹H NMR (400 MHz, MeOD- d_4) δ : 8.23 (d, 1H, $J=8.0$ Hz, H-8), 7.62 – 7.68 (m, 2H, H-5 & H-6), 7.43 (t, 1H, $J=8.0$ Hz, H-7), 7.37 (s, 1H, H-3') 7.24 – 7.25 (m, 2H, H-4' & H-5'), 7.02 (d, 1H, $J=8.0$ Hz, H-6'), 3.99 (s, 3H, OCH₃), 3.80 (t, 2H, $J=8.0$ Hz, CH₂NH), 3.43 (t, 2H, $J=8.0$ Hz, CH₂NHCO), 2.93 (brs, 2H, H-4), 2.71 (brs, 2H, H-1), 1.90 (brs, 4H, H-2 & H-3), 1.73–1.86 (m, 4H, NHCH₂CH₂CH₂); ¹³C NMR (100 MHz, MeOD- d_4) δ : 159.66, 154.03, 148.57, 145.71, 144.42, 142.40, 130.36, 128.93, 124.30, 124.12, 123.95, 117.86, 114.09, 113.62, 109.99, 108.37, 55.05, 38.53, 30.33, 27.77, 26.15, 24.06, 22.10, 21.30; HRMS (ESI) calcd for C₂₇H₃₀N₃O₃⁺ [M + H]⁺, m/z 444.2282, found 444.2260.

4.2.17. *N*-(3-((6-chloro-1,2,3,4-tetrahydroacridin-9-yl)amino)propyl)-7-methoxybenzofuran-2-carboxamide (19)

The title compound was synthesised from the reaction of compounds **4** and **11**. Yield 70%; mp 157 – 158 °C. ¹H NMR (400 MHz, MeOD- d_4) δ : 8.35 (d, 1H, $J=8.0$ Hz, H-8), 7.62 (s, 1H, H-5), 7.48 (d,

1H, $J=8.0$ Hz, H-4'), 7.35 (s, 1H, H-3'), 7.27 (brs, 2H, H-7 & H-5'), 7.05 (m, 1H, H-6'), 4.08 (brs, 2H, $\overline{CH_2NH}$), 4.01 (s, 3H, OCH₃), 3.58 (brs, 2H, $\overline{CH_2NHCO}$), 2.87 (brs, 2H, $\overline{H-4}$), 2.71 (brs, 2H, H-1), 2.17 (m, 2H, $\overline{NHCH_2CH_2}$) 1.90 (brs, 4H, H-2 & H-3); ¹³C NMR (100 MHz, MeOD-*d*₄) δ : 159.87, 156.56, 150.68, 148.24, 145.68, 144.39, 139.00, 138.55, 128.81, 127.11, 125.28, 124.44, 117.61, 114.11, 113.99, 112.09, 110.18, 108.52, 55.06, 45.18, 36.02, 29.52, 27.84, 23.40, 21.38, 20.22; HRMS (ESI) calcd for C₂₆H₂₇ClN₃O₃ [M + H]⁺, m/z 464.6577, found 464.6565.

4.2.18. *N*-(4-((6-chloro-1,2,3,4-tetrahydroacridin-9-yl)amino)butyl)-7-methoxybenzofuran-2-carboxamide (20)

The title compound was synthesised from the reaction of compounds **4** and **12**. Yield 79%; mp 245 – 247 °C. ¹H NMR (400 MHz, MeOD-*d*₄) δ : 8.39 (d, 1H, $J=8.0$ Hz, H-8), 7.51 – 7.52 (m, 2H, H-5 & H-4'), 7.33 (s, 1H, H-3'), 7.28 – 7.29 (m, 2H, H-7 & H-5'), 7.05 – 7.07 (m, 1H, H-6'), 4.05 (t, 2H, $J=8.0$ Hz, $\overline{CH_2NH}$), 4.01 (s, 3H, OCH₃), 3.45 (t, 2H, $J=8.0$ Hz, $\overline{CH_2NHCO}$), 2.91 (brs, 2H, H-4), 2.69 (brs, 2H, H-1), 1.96–1.97 (m, 6H, $\overline{NHCH_2CH_2}$, H-2 & H-3), (m, 2H, $\overline{CH_2CH_2NHCO}$); ¹³C NMR (100 MHz, MeOD-*d*₄) δ : 159.55, 156.17, 150.66, 148.45, 145.66, 144.32, 140.16, 138.43, 128.84, 127.27, 125.30, 124.40, 117.85, 114.08, 112.39, 109.93, 108.42, 55.04, 38.49, 28.11, 27.09, 25.45, 23.24, 21.45, 20.35; HRMS (ESI) calcd for C₂₇H₂₉ClN₃O₃ [M + H]⁺, m/z 478.6745, found 478.6734.

4.2.19. General procedure for the deprotection of the hydroxy group (21–24)

A mixture of 7-methoxy-*N*-(4-((1,2,3,4-tetrahydroacridin-9-yl)amino)alkyl)-benzofuran-2-carboxamide (1 eq.) and *n*-Bu₄NI (3 eq.) in dry CH₂Cl₂ (15 mL) was stirred under N₂ atmosphere and cooled to –78 °C. To this solution was dropwise added an excess of a solution 1 M BCl₃ in CH₂Cl₂ (5 eq.). After ca 5 min, the solution could warm to room temperature and was stirred for 2 h. The reaction was quenched with ice water and it was left to stir for 30 min. A precipitate was formed and the product was recrystallized from CH₃CN/Et₂O to afford the pure final compounds as a pale yellow solids. Yield: 40 – 66%.

4.2.20. 7-Hydroxy-*N*-(3-((1,2,3,4-tetrahydroacridin-9-yl)amino)propyl)benzofuran-2-carboxamide (21)

The title compound was synthesised from compound **17**. Yield 40%; mp 93 – 95 °C. ¹H NMR (400 MHz, MeOD-*d*₄) δ : 8.28 (d, 1H, $J=8.0$ Hz, H-8), 7.62 – 7.70 (m, 2H, H-5 & H-6), 7.45 (t, 1H, $J=8.0$ Hz, H-7), 7.33 (s, 1H, H-3') 7.19–7.20 (m, 2H, H-4' & H-5'), 6.96–6.97 (m, 1H, H-6'), 3.98 (t, 2H, $J=8.0$ Hz, $\overline{CH_2NH}$), 3.52–3.53 (m, 2H, $\overline{CH_2NHCO}$), 2.85 (brs, 2H, H-4), 2.66 (brs, 2H, H-1), 2.08–2.13 (m, 2H, $\overline{NHCH_2CH_2}$) 1.84 (brs, 4H, H-2 & H-3); ¹³C NMR (100 MHz, MeOD-*d*₄) δ : 159.98, 156.02, 150.85, 148.32, 145.67, 144.40, 138.99, 132.08, 128.84, 124.72, 124.37, 119.34, 115.94, 114.08, 111.84, 110.17, 55.07, 45.00, 36.15, 29.95, 28.27, 23.64, 21.60, 20.47. HRMS (ESI) calcd for C₂₅H₂₅N₃O₃⁺[M + H]⁺, m/z 415.1904, found 415.1951.

4.2.21. 7-Hydroxy-*N*-(4-((1,2,3,4-tetrahydroacridin-9-yl)amino)butyl)benzofuran-2-carboxamide (22)

The title compound was synthesised from **18**. Yield 50%; mp 79 – 81 °C. ¹H NMR (400 MHz, MeOD-*d*₄) δ : 8.23 (d, 1H, $J=8.0$ Hz, H-8), 7.62–7.68 (m, 2H, H-5 & H-6), 7.43 (t, 1H, $J=8.0$ Hz, H-7), 7.37 (s, 1H, H-3'), 7.24–7.25 (m, 2H, H-4' & H-5'), 7.02 (d, 1H, $J=8.0$ Hz,

H-6'), 3.80 (t, 2H, $J=8.0$ Hz, $\overline{CH_2NH}$), 3.43 (t, 2H, $J=8.0$ Hz, $\overline{CH_2NHCO}$), 2.93 (brs, 2H, H-4), 2.71 (brs, 2H, H-1), 1.90 (brs, 4H, H-2 & H-3), 1.73–1.86 (m, 4H, $\overline{NHCH_2CH_2CH_2}$); ¹³C NMR (100 MHz, MeOD-*d*₄) δ : 159.66, 154.03, 148.57, 145.71, 144.42, 142.40, 130.36, 128.93, 124.30, 124.12, 123.95, 117.86, 114.09, 113.62, 109.99, 55.05, 38.53, 30.33, 27.77, 26.15, 24.06, 22.10, 21.30. HRMS (ESI) calcd for C₂₆H₂₇N₃O₃ [M + H]⁺, m/z 429.2058, found 429.2083.

4.2.22. *N*-(3-((6-chloro-1,2,3,4-tetrahydroacridin-9-yl)amino)propyl)-7-hydroxybenzofuran-2-carboxamide (23)

The title compound was synthesised from compound **19**. Yield 50%; mp 85 – 87 °C. ¹H NMR (400 MHz, MeOD-*d*₄) δ : 8.35 (d, 1H, $J=8.0$ Hz, H-8), 7.62 (s, 1H, H-5), 7.48 (d, 1H, $J=8.0$ Hz, H-4'), 7.35 (s, 1H, H-3'), 7.27 (brs, 2H, H-7 & H-5'), 7.05 (m, 1H, H-6'), 4.08 (brs, 2H, $\overline{CH_2NH}$), 4.01 (s, 3H, OCH₃), 3.58 (brs, 2H, $\overline{CH_2NHCO}$), 2.87 (brs, 2H, $\overline{H-4}$), 2.71 (brs, 2H, H-1), 2.17 (m, 2H, $\overline{NHCH_2CH_2}$) 1.90 (brs, 4H, H-2 & H-3); ¹³C NMR (100 MHz, MeOD-*d*₄) δ : 159.87, 156.56, 150.68, 148.24, 145.68, 144.39, 139.00, 138.55, 128.81, 127.11, 125.28, 124.44, 117.61, 114.11, 113.99, 112.09, 110.18, 55.06, 45.18, 36.02, 29.52, 27.84, 23.40, 21.38, 20.22. HRMS (ESI) calcd for C₂₅H₂₅ClN₃O₃ [M + H]⁺, m/z 450.6442, found 450.6450.

4.2.23. *N*-(4-((6-chloro-1,2,3,4-tetrahydroacridin-9-yl)amino)butyl)-7-hydroxybenzofuran-2-carboxamide (24)

The title compound was synthesised from compound **20**. Yield 66%; mp 100 – 101 °C; ¹H NMR (400 MHz, MeOD-*d*₄) δ : 8.39 (d, 1H, $J=8.0$ Hz, H-8), 7.51 – 7.52 (m, 2H, H-5 & H-4'), 7.33 (s, 1H, H-3'), 7.28 – 7.29 (m, 2H, H-7 & H-5'), 7.05 – 7.07 (m, 1H, H-6'), 4.05 (t, 2H, $J=8.0$ Hz, $\overline{CH_2NH}$), 3.45 (t, 2H, $J=8.0$ Hz, $\overline{CH_2NHCO}$), 2.91 (brs, 2H, H-4), 2.69 (brs, 2H, H-1), 1.96–1.97 (m, 6H, $\overline{NHCH_2CH_2}$, H-2 & H-3), (m, 2H, $\overline{CH_2CH_2NHCO}$); ¹³C NMR (100 MHz, MeOD-*d*₄) δ : 159.55, 156.17, 150.66, 148.45, 145.66, 144.32, 140.16, 138.43, 128.84, 127.27, 125.30, 124.40, 117.85, 114.08, 112.39, 109.93, 55.04, 38.49, 28.11, 27.09, 25.45, 23.24, 21.45, 20.35. HRMS (ESI) calcd for C₂₆H₂₆ClN₃O₃ [M + H]⁺, m/z , 464.6511, found 463.6498.

4.3. Molecular modelling

The interactions between ligands and proteins are of fundamental importance in the modern structure-based drug design, and so docking simulations with GOLD v. 5.1 program⁴³ were performed. The inhibitor models were docked inside the protein model of *Torpedo californica* AChE (*TcAChE*), which was obtained from the X-ray structure of its complex with an AChE inhibitor (*N*-4'-quinolyl-*N'*-9''-(1'',2'',3'',4''-tetrahydroacridinyl)-1,8-diaminooctane, herein called original ligand), retrieved from the RCSB Protein Data Bank (PDB entry 1ODC)²⁰. This structure was chosen due to the similarity between this ligand and the herein studied ligands, namely the TAC and the aromatic moiety linked by an alkylic chain, interacting respectively with the catalytic active site (CAS) and the peripheral anionic site (PAS). Structures from *Homo sapiens* were not selected because they are complexed with smaller inhibitors. To get the protein model, the original complex model was treated with the programme MAESTRO v. 9.3⁴⁴ by removal of the original ligand, solvent and co-crystallized molecules, as well as by addition of hydrogen atoms. This programme was also used to design the ligand structures, which afterwards were optimised with software GHEMICAL v. 2.0⁴⁵, through a random conformational search of 100 cycles and 2500 optimisation steps. To complete these simulations, the ligand models were docked inside the active site of the AChE structure through the programme GOLD v. 5.1, using its

standard parameters and the Astex Statistical Potential (ASP) scoring function. The zone of interest of the docking was defined as the residues within 10 Å from the original position of the ligand in the crystal structure. The docking protocol used herein was validated, through the re-docking of the co-crystallized ligand (original ligand)²⁰ into the respective AChE model, leading to a structure with very good superimposition to that of reported X-ray crystal structure, as recently reported.¹⁶

4.3.1. Prediction of pharmacokinetic properties

To get an insight on drug-likeness properties of these new hybrids, *in silico* calculations of some pharmacokinetic descriptors were performed by the QikProp program³⁹ provided by MAESTRO. Parameters such as the lipo-hydrophilic character (clog *P*), blood-brain barrier partition coefficient (log BB), ability to be absorbed through the intestinal tract (Caco-2 cell permeability) and CNS activity were calculated. These predictions are for orally delivered drugs and assume non active transport.

4.4. Physico-chemical properties

4.4.1. Anti-oxidant activity

The anti-oxidant capacity or, more precisely, radical scavenging activity based on the electron and proton donation ability, was evaluated by the DPPH method previously described^{29,46}. To a 2.5 mL solution of DPPH (0.002%) in methanol, solutions of each compound were added in different volumes to obtain different concentrations in a 3.5 mL final volume. The samples were incubated for 30 min at room temperature. The absorbance was measured at 517 nm against the corresponding blank (methanol). The antioxidant activity was calculated by Eq. (1)²⁹.

$$\%AA = ((A_{DPPH} - A_{sample}) / A_{DPPH}) \times 100 \quad (1)$$

The tests were carried out in triplicate. The compound concentration providing 50% of antioxidant activity (EC₅₀) was obtained by plotting the antioxidant activity against the compound concentration.

4.4.2. Metal chelation studies

The metal-complexation studies of compound **21** were performed by UV-Vis spectroscopic titration. Due to solubility reasons, these equilibrium solution studies were accomplished in a mixed 25% (w/w) DMSO/water medium, at $T = 25.0 \pm 0.1$ °C and ionic strength (*I*) 0.1 M KCl. The glass and Ag/AgCl reference electrodes were previously conditioned in different DMSO/H₂O mixtures of increasing DMSO % composition and the response of the glass electrode was checked by strong acid – strong base (HCl/KOH) calibrations and analysis of the respective Nernst parameters by Gran's method⁴⁷. For the spectrophotometric titrations (total volume 30 mL), the ligand concentration (*C_L*) was 4.0×10^{-5} M and *C_M*/*C_L* ratios of 0:1, 1:1 (M = Cu, Fe), 1:2 (M = Cu) and 1:3 (M = Fe) were used. The spectrophotometric measurements were carried out in a 280–450 nm wavelength range at pH ca 2.4–10. The value determined for the water ionisation constant (*pK_w*) was 14.40. The step-wise protonation constants of the ligand, $K_i = [H_iL] / [H_{i-1}L][H]$ (*i* = 1–2), and the overall metal-complex stability constants, $\beta_{M_mH_hL_l} = [M_mH_hL_l] / [M]^m[H]^h[L]^l$, were calculated by fitting the spectrophotometric data with PSEQUAD program⁴⁸. The Fe(III) and Cu(II) hydrolysis models were determined under the defined experimental conditions (*I* = 0.1 M KCl, 25% w/w DMSO/H₂O, $T = 25.0 \pm 0.1$ °C) and the following values of stability constants

were included in the fitting of experimental data towards the equilibrium models related to the Fe(III)/L and Cu(II)/L systems: log $\beta_{FeH-2} = -6.78$, log $\beta_{FeH-3} = -10.78$; log $\beta_{CuH-2} = -9.94$. The species distribution curves were obtained with the Hyss program⁴⁷.

4.5. Acetylcholinesterase inhibition

The enzymatic activity of AChE was determined using an adaptation of the Ellman's method, as described previously^{29,32}. Firstly, a stock solution of AChE was prepared by dissolving enzyme 500 U in 10 mL of tris(hydroxymethyl)aminomethane (TRIS) buffer (50 mM, pH 8). Then, 4-(2-hydroxyethyl)-1-piperazineethanesulfonic acid (HEPES) buffer was used for further dilution of the enzyme solution therefore obtaining the final working solution of AChE. The assay solution consisted of 374 μL of HEPES buffer (50 mM and pH 8.0), a variable volume (10–50 μL) of the compound's stock solution (1 mg/mL of MeOH), 476 μL of 3 mM bis(3-carboxy-4-nitrophenyl) disulphide (DTNB), 25 μL of AChE stock solution and the necessary amount of methanol to attain the same volume of sample mixture in a 1 mL cuvette. After mixing, samples were left to incubate for 15 min and then 75 μL of 16 mM acetylthiocholine iodide (AChI) solution was added and immediately the reaction was monitored at 405 nm for 5 min. Firstly, enzyme activity was determined by measuring the rate of enzymatic reaction in solution by recording absorbance (with or without enzyme) at 405 nm. To calculate the percent inhibition of AChE, the enzyme activity in the presence of increasing concentrations of the test compound, as well as for a blank reaction (methanol without compounds), were measured at 405 nm.

The obtained results were expressed in percentage of inhibition through the Equation (2):

$$\%I = 100 - (v_1 / v_0 \times 100) \quad (2)$$

Where *v₁* is the initial reaction rate in the presence of the inhibitor and *v₀* is the initial rate of the control reaction. The curves of inhibition were obtained using a plot of percentage of enzymatic inhibition versus inhibitor concentration, and a calibration curve was obtained from which the linear regression parameters were obtained.

4.6. Inhibition of self-mediated and Cu²⁺ induced Aβ₁₋₄₂ aggregation

Among all the methods to measure the aggregation of Aβ₁₋₄₂, the assay based on Thioflavin T (ThT) is the standard procedure based on the fluorescence of this dye^{49,50}. This test is performed with Aβ₁₋₄₂ peptide previously prepared by dissolving it in 1,1,1,3,3,3-hexafluoro-2-propanol (HFIP), an organic solvent useful to solubilise and monomerize the β-sheet protein aggregates and reserve them in the fridge. Films are re-dissolved in an Eppendorf tube with a fresh solution of a mixture of CH₃CN/Na₂CO₃/NaOH, to have a stable stock solution, and afterwards, added to an optimised fibrillation phosphate buffer¹⁴. The samples were prepared using MeOH (1 mg/mL) as solvent, followed by incubation in a water bath for 24 h at 37 °C with gentle shaking. After incubation, the samples were added to a 96-well plate (BD Falcon) with 180 μL of 5 μM ThT in 50 mM glycine-NaOH (pH 8.5) buffer. Blank samples were prepared for each concentration in a similar way, devoid of peptide. After 5-min incubation with the dye, the ThT fluorescence was measured at 446 nm (excitation) and 485 nm (emission).

4.7. Transmission electron microscopy (TEM)

The Transmission Electron Microscopy (TEM) is a high resolution technique used to study biological or inorganic samples at 2–3 nm level, through black and white high-quality images. The compound **21** was selected among those with better anti- $A\beta$ aggregation assay. Imaging acquisition was performed with samples of the ligand mixed with $A\beta$, in the absence or presence of copper, prepared by following the single-droplet method in the negative staining protocol. The $A\beta$ stock solutions were prepared by dissolving the lyophilised peptide in a mixture of 48 μ L of CH_3CN , 10 μ L of NH_4OH (2%) and 48 μ L of NaCl (300 μ M), followed by addition of a buffered solution containing 4-(2-hydroxyethyl)-1-piperazine-ethanesulfonic acid (HEPES, 50 mM, pH = 6.6) to obtain a total concentration of 50 μ M. The ligands were treated with amyloid- β peptide and prepared previously to be studied in absence or in presence of copper chloride (25 μ M) and everything was followed by incubation for 24 h at 37 °C. Formvar/Carbon 200-mesh Cu grids (Ted Pella) were treated with $A\beta$ peptide aggregated samples (10 μ L) for 2 min at rt. Excess sample solution was removed using filter paper followed by washing twice with deionised water. Each grid incubated with uranyl acetate (1%, 10 μ L, 1 min) was stained and dried for 15 min at rt. The support device used to hold the sample inside TEM was a copolymer of polyvinyl acetate from polyvinyl alcohol and formaldehyde called *Formvar* stabilised with a thin layer of carbon, using copper 200 – mesh grids as a main support (purchased to Ted Pella).

4.8. Cell viability and neuroprotection

SH-SY5Y human neuroblastoma cell line (ATCC-CRL-2266) is grown in Dulbecco's modified Eagle's medium (DMEM), and were obtained from Gibco-Invitrogen (Life Technologies Ltd, UK) with 10% heat inactivated foetal calf serum, containing 50 U/mL penicillin and 50 μ g/mL streptomycin, under a humidified atmosphere of 95% air- 5% CO_2 at 37 °C. Cells were plated at 0.12×10^6 cells/mL for cell viability assay. The tested compounds (**18**, **19**, **20**, **21**, **23** and **24**) were dissolved in DMSO at a concentration of 50 mM and aliquots were stored at –20 °C. We performed a dose-response screening (from 10 μ M to 40 μ M) in order to choose the highest non-toxic concentration. As a result we selected: 20 μ M final concentrations for compounds **18**, **19**, **20** and **23**; 20 μ M final concentration for compound **19**; 35 μ M final concentration for compounds **21** and **24**. The final concentration of DMSO in culture media did not exceed 0.05% (v/v) and no alterations on cells were observed. The compounds were added to the cell media 1 h before the incubation with $A\beta_{1-42}$ or L-ascorbic acid/ferrous sulphate. $A\beta_{1-42}$ or L-ascorbic acid/ferrous sulphate were incubated alone or with the compound for an additional 24 h. $A\beta_{1-42}$ was prepared as 276.9 μ M stock in sterile water and added to the medium at 2.5 μ M final concentration. Ferrous sulphate was freshly prepared as 0.36 M stock in water and added to the medium at 500 μ M final concentration. L-Ascorbic Acid was freshly prepared as 80 mM stock in water and added to the medium at 5 mM final concentration. $A\beta_{1-42}$ was purchased from Bachem (Torrance, CA, USA) and ferrous sulphate and L-ascorbic acid from Sigma Chemical Co (St. Louis, MO, USA).

Cell viability was determined by the MTT (3-(4,5-dimethylthiazol-2-yl)-2,5-diphenyltetrazolium bromide) reduction test. In viable cells, the enzyme succinate dehydrogenase metabolises MTT into a formazan that absorbs light at 570 nm. Following the cell treatment protocol, the medium was aspirated and 0.5 mL MTT (0.5 mg/mL) was added to each well. The plate was then

incubated at 37 °C for 1 h 30 min protected from light. At the end of the incubation period, the formazan precipitates were solubilised with 0.5 mL of acidic isopropanol (0.04 M HCl/isopropanol). The absorbance was measured at 570 nm⁵¹. Cell reduction ability was expressed as a percentage of untreated control cells.

All data were expressed as mean \pm SEM of at least three independent experiments performed in duplicates. Statistical analyses were performed using GraphPad Prism 5 (GraphPad Software, San Diego, CA, USA). Differences between two datasets were evaluated by two-tailed unpaired Student's t test A *p*-value <0.05 was considered statistically significant.

Acknowledgements

The authors thank the Portuguese *Fundação para a Ciência e Tecnologia* (FCT), for the financial support of the projects UID/QUI/00100/2013, UID/QUI/00100/2019, the postdoctoral fellowship (KC), and also thank the Erasmus⁺ programme (GF). Acknowledgements are also due to the Portuguese NMR (IST-UL Center) and Mass Spectrometry Networks (Grant LISBOA-01–0145-FEDER-022125).

Disclosure statement

No potential conflict of interest was reported by the authors.

ORCID

Gaia Fancellu  <http://orcid.org/0000-0002-9705-3779>
 Karam Chand  <http://orcid.org/0000-0001-7691-4392>
 Daniel Tomás  <http://orcid.org/0000-0002-9000-0535>
 Elisabetta Orlandini  <http://orcid.org/0000-0003-3398-2787>
 Luca Piemontese  <http://orcid.org/0000-0002-7980-5818>
 Diana F. Silva  <http://orcid.org/0000-0002-0612-2645>
 Sandra M. Cardoso  <http://orcid.org/0000-0002-2199-0555>
 Sílvia Chaves  <http://orcid.org/0000-0002-8554-4992>
 M. Amélia Santos  <http://orcid.org/0000-0002-4069-9368>

References

1. a) Alzheimer's Association, Alzheimer's disease facts and figures, Alzheimer's Dement. J Alzheimer's Assoc 2017;13: 325–73.; b) W.H. Organization in: The Global Dementia Observatory Reference Guide, World Health Organization. 2018; <http://www.who.int/iris/handle/10665/272669>.
2. Lillo-Crespo M, Riquelme J, Macrae R, et al. Experiences of advanced dementia care in seven European countries: implications for educating the workforce. Glob Health Action 2018;11:1478686.
3. Scheff SW, Price DA, Schmitt FA, et al. Hippocampal synaptic loss in early Alzheimer's disease and mild cognitive impairment. Neurobiol Aging 2006;27:1372–84.
4. Bloom GS. Amyloid- β and tau: the trigger and bullet in Alzheimer disease pathogenesis. JAMA Neurol 2014;71: 505–8.
5. Marco-Contelles J. Facts, results, and perspectives of the current Alzheimer's disease research. ACS Chem Neurosci 2019; 10:1127–8.
6. Tricco AC, Ashoor HM, Soobiah C, et al. Comparative effectiveness and safety of cognitive enhancers for treating Alzheimer's disease: systematic review and network meta-analysis. J Am Geriatr Soc 2018;66:170–8.

7. a) Panza F, Seripa D, Lozupone M, et al. The potential of solanezumab and gantenerumab to prevent Alzheimer's disease in people with inherited mutations that cause its early onset. *Expert Opin Biol Ther* 2018;18:25–35; b) Rinaldi A. Setbacks and promises for drugs against Alzheimer's disease: as pharmaceutical companies are retreating from drug development for Alzheimer's, new approaches are being tested in academia and biotech companies. *EMBO Rep* 2018; 19:e46714.
8. Guziar N, Ckowska AW, Panek D, et al. Recent development of multifunctional agents as potential drug candidates for the treatment of Alzheimer's disease. *Curr Med Chem* 2014; 22:373–404.
9. Ramsay RR, Popovic-Nikolic MR, Nikolic K, et al. A perspective on multi-target drug discovery and design for complex diseases. *Clin Trans Med* 2018;7:3.
10. Oset-Gasque MJ, Marco-Contelles J. Alzheimer's Disease, the "One-Molecule, One-Target" Paradigm, and the multitarget directed ligand approach. *ACS Chem Neurosci* 2018;9:401–3.
11. Santos MA, Chand K, Chaves S. Recent progress in repositioning Alzheimer's disease drugs based on a multitarget strategy. *Fut Med Chem* 2016;8:2113–42.
12. Girek M, Szymański P. Tacrine hybrids as multi-target-directed ligands in Alzheimer's disease: influence of chemical structures on biological activities. *Chem Papers* 2019;73: 269–89.
13. Pérez-Areales FJ, Turcu AL, Barniol-Xicota M, et al. A novel class of multitarget anti-Alzheimer benzohomoadamantane–chlorotacrine hybrids modulating cholinesterases and glutamate NMDA receptors. *Eur J Med Chem* 2019;180: 613–626; b) Chalupova K, Korabecny J, Bartolini M, et al. Novel tacrine-tryptophan hybrids: Multi-target directed ligands as potential treatment for Alzheimer's disease. *Eur J Med Chem* 2019;168:491–514.
14. Hiremathad A, Keri RS, Esteves AR, et al. Novel tacrine-hydroxyphenylbenzimidazole hybrids as potential multitarget drug candidates for Alzheimer's disease. *Eur J Med Chem* 2018;148:255–67.
15. Piemontese L, Tomás D, Hiremathad A, et al. Donepezil structure-based hybrids as potential multifunctional anti-Alzheimer's drug candidates. *J Enz Inhib Med Chem* 2018;33: 1212–24.
16. a) Chand K, Rajeshwari, Chaves S, et al. Tacrine–deferiprone hybrids as multi-target-directed metal chelators against Alzheimer's disease: a two-in-one drug. *Metallomics*, 2018; 10:1460–5.; b) Rajeshwari, Chand K, Candeias E, et al. New multitarget hybrids bearing tacrine and phenylbenzothiazole motifs as potential drug candidates for Alzheimer's disease. *Molecules* 2019;24:587–601.
17. Chand K, Rajeshwari HA, et al. A review on antioxidant potential of bioactive heterocycle benzofuran: Natural and synthetic derivatives. *Pharmacol Rep* 2017;69:281–95.
18. a) Goyal D, Kaur A, Goyal B. Benzofuran and indole: Promising scaffolds for drug development in Alzheimer's disease. *Chem Med Chem* 2018;13:1275–99.; b) Paudel P, Seong SH, Zhou Y, et al. Arylbenzofurans from the Root Bark of *Morus alba* as Triple Inhibitors of Cholinesterase, β -Site Amyloid Precursor Protein Cleaving Enzyme 1, and Glycogen Synthase Kinase-3 β : Relevance to Alzheimer's Disease. *ACS Omega* 2019;4:6283–6294.
19. Hiremathad A, Chand K, Tolayan L, et al. Hydroxypyridinone-benzofuran hybrids with potential protective roles for Alzheimer's disease therapy. *J Inorg Biochem* 2018;179: 82–96.
20. PDB Protein Data Base, entry 1ODC, <http://www.rcsb.org/structure/1ODC>.
21. Cheung J, Rudolph MJ, Burshteyn F, et al. Structures of human acetylcholinesterase in complex with pharmacologically important ligands. *J Med Chem* 2012;55:10282–6.
22. Dvir H, Silman I, Harel M, et al. Acetylcholinesterase: from 3D structure to function. *Chem Biol Interact* 2010;187:10–22.
23. Ceshi MA, Costa JS, Lopes JPB, et al. Novel series of tacrine-tianeptine hybrids: Synthesis, cholinesterase inhibitory activity, S100B secretion and a molecular modeling approach. *Eur J Med Chem* 2016;121:758–72.
24. Campos P, Formosa X, Galdeano C, et al. Tacrine-based dual binding site acetylcholinesterase inhibitors as potential disease-modifying anti-Alzheimer drug candidates. *Chem Biol Interact* 2010;187:411–515.
25. Zha X, Lamba D, Zhang L, et al. Novel tacrine – benzofuran hybrids as potent multitarget-directed ligands for the treatment of Alzheimer's disease: design, synthesis, biological evaluation, and X-ray crystallography. *J Med Chem* 2016;59: 114–31.
26. Keri RS, Quintanova C, Chaves S, et al. New tacrine hybrids with natural based cysteine derivatives as multi-targeted drugs for potential treatment of Alzheimer's disease. *Chem Biol Drug Des* 2016;87:101–11.
27. Brooks PR, Wirtz MC, Vetelino MG, et al. Boron trichloride/tetra-n-butylammonium iodide: a mild, selective combination reagent for the cleavage of primary alkyl aryl ethers. *J Org Chem* 1999;64:9719–21.
28. Quintanova C, Keri RS, Marques SM, et al. Design, synthesis and bioevaluation of tacrine-cinnamate based hybrids as potential bifunctional anti-Alzheimer drug candidates. *Med Chem Comm* 2015;6:1969–77.
29. Sebestík J, Marques SM, Falé PL, et al. Bifunctional phenolic-choline conjugates as anti-oxidants and acetylcholinesterase inhibitors. *J Enz Inhib Med Chem* 2011;26:485–97.
30. Marques SM, Abate CC, Chaves S, et al. New bifunctional metalloproteinase inhibitors: an integrated approach towards biological improvements and cancer therapy. *J Inorg Biochem* 2013;127:188–202.
31. Chaves S, Hiremathad A, Tomás D, et al. Exploring the chelating capacity of 2-hydroxyphenylbenzimidazole based hybrids with multi-target ability as anti-Alzheimer's agents. *New J Chem* 2018;42:16503–15.
32. Ellman GL, Courtney KD, Andres V, Jr, et al. A new and rapid colorimetric determination of acetylcholinesterase activity. *Biochem Pharmacol* 1961;7:88–95.
33. Seeman P, Seeman N. Alzheimer's disease: β -amyloid plaque formation in human brain. *Synapse* 2011;65:1289–97.
34. Gleichmann M, Mattson MP. Alzheimer's disease and neuronal network activity. *Neuromol Med* 2010;12:44–7.
35. Hudson SA, Ecroyd H, Kee TW, et al. The thioflavin T fluorescence assay for amyloid fibril detection can be biased by the presence of exogenous compounds. *FEBS J* 2009;276: 5960–72.
36. Biancalana M, Koide S. Molecular mechanism of Thioflavin-T binding to amyloid fibrils. *Biochim Biophys Acta* 2010;1804: 1405–12.
37. Gestwicki JE, Ranke A. Structure-activity relationships of amyloid beta-aggregation inhibitors based on curcumin: influence of linker length and flexibility. *Chem Biol Drug Des* 2007;70:206–15.

38. Jones MR, Service EL, Thompson JR, et al. Dual-function triazole-pyridine derivatives as inhibitors of metal-induced amyloid- β aggregation. *Metallomics* 2012;4:910–20.
39. QikProp, version 2.5, Schrödinger. New York: LLC; 2005.
40. Cheignon C, Tomas M, Bonnefont-Rousselot DP, et al. Oxidative stress and the amyloid beta peptide in Alzheimer's disease. *Redox Biol* 2018;14:450–64.
41. Armarego WLF, Perring DD (Eds). *Purification of laboratory chemicals*. 4th ed. Oxford: Butterworth-Heinemann Press; 1999.
42. Rossotti FJC, Rossotti H. H. Potentiometric titrations using Gran plots: A textbook omission. *J Chem Ed* 1965;42:375–8.
43. Taylor RD, Jewsbury PJ, Essex PJ. A review of protein-small molecule docking methods. *J Comp-Aided Mol Des* 2002;16:151–66.
44. Maestro, Version 9.3, Portland: Schrödinger Inc; 2012.
45. Hassinen T, Peräkylä MJ. New energy terms for reduced protein models implemented in an off-lattice force field. *Comput Chem* 2001;22:1229–42.
46. Tepe B, Daferera D, Sokmen A, et al. Antimicrobial and antioxidant activities of the essential oil and various extracts of *Salvia tomentosa* Miller (Lamiaceae). *J Agric Food Chem* 2005;90:333–40.
47. Gans P, Sabatini A, Vacca A. Investigation of equilibria in solution. Determination of equilibrium constants with the HYPERQUAD suite of programs. *Talanta* 1996;43:1739–53.
48. Zékány L, Nagypál I, Peintler G. PSEQUAD for Chemical Equilibria, Update 5.01; 2001.
49. Bartolini M, Bertucci C, Bolognesi ML, et al. Insight into the kinetic of amyloid beta (1-42) peptide self-aggregation: elucidation of inhibitors' mechanism of action. *ChembioChem* 2007;8:2152–61.
50. Chao X, He X, Yang Y, et al. Design, synthesis and pharmacological evaluation of novel tacrine-caffeic acid hybrids as multi-targeted compounds against Alzheimer's disease. *Bioorg Med Chem Lett* 2012;22:6498–502.
51. Mosmann T. Rapid colorimetric assay for cellular growth and survival: application to proliferation and cytotoxicity assays. *J Immunol Methods* 1983;65:55–63.